SOS-Water deliverable report

D2.2: Established linkages between WSMs and IMs and building and benchmarking IWMS

Lead beneficiary	2 - UU	Due Date	30/09/2024
WP no	2	New due date (if delay)	
Task no	2	Actual Delivery Date	25/09/2024
Dissemination level	PU – Public	Status	Submitted

Authors

Authors	Partner no	Partner organization	Name of author
Main author	2	Utrecht University	Niko Wanders Jennie Steyaert
Contributing author(s)	1	IIASA	Emilio Politti Peter Burek Carla Catania Silvia Artuso
	4	POLIMI	Bruno Invernizzi Teresa Bonserio Giorgio Guariso Wei Xia Matteo Giuliani Andrea Castelletti
	5	FVB-IGB	Sami Domisch Jaime García
	8	SIWRP	Dang Thanh Lam Nguyen Van Phuong Nguyen Thi Phuong
	3	UPV	Hector Macian-Sorribes

Review

Authors	Partner no	Partner organization	Name of author
Technical review	6	FutureWater	Gijs Simons
Language review – *if applicable*			

Document history

Date	Version	Chapters affected	Description of change	Author	Document status
19/08/2024	0.1	All	Outline	Niko Wanders, Jennie Steyaert	DRAFT
02/09/2024	0.2	All	First draft	Niko Wanders, Jennie Steyaert Emilio Politti Peter Burek Carla Catania Silvia Artuso Bruno Invernizzi Teresa Bonserio Giorgio Guariso Wei Xia Matteo Giuliani Andrea Castelletti Sami Domisch Jaime García Dang Thanh Lam Nguyen Van Phuong Nguyen Thi Phuong Hector Macian-Sorribes	DRAFT
09/09/2024	0.3	All	Technical Review	Gijs Simons	DRAFT
23/09/2024	0.4	All	Final Draft	Niko Wanders, Jennie Steyaert Taher Kahil	DRAFT
25/09/2024	1	All	Finalisation & formatting	Alberto Fresolone Silvia Artuso	FINAL
22/01/2026	2.0	All	Review of deliverable based on reviewers' feedback	All from the final list above	FINAL

29/01/2026	2.1	All	Deliverable revised based on reviewers' feedback	Niko Wanders, Jennie Steyaert	FINAL

Publishable Executive Summary

This deliverable describes how linkages are established between the water system models (PCRGLOBWB 2, CWatM, VRSAP, and Vic-Res) and the impact models (D-CASCADE, biodiversity model, hydro-economic model) used in the SOS-Water project. These model connections are benchmarked against well-established observational datasets. The document starts with describing the different case study regions and which water system models have been deployed for each case study region. It describes the biodiversity impact models used to quantify the hydrological regime's impact on biodiversity. This is followed by the results section that describes the improvements that have been made to the water system models and how these model results compare to the observational data.

Within SOS-Water we have used a wide variety of well-established water system models that have been deployed in other studies around the world and are internationally recognized to be state-of-the-art when it comes to large-scale hydrological modelling. The CWatM model is used for the simulations of the Danube, the PCR-GLOBWB 2 model is used for the simulations for the Rhine, the Mekong is simulated using Mike11- ST and Vic-Res and finally a hydroeconomic model developed by UPV is used to model the Jucar River basin. The impact models are covered by a species distribution model for biodiversity impact assessment and a combined VIC-Res and D-CASCADE model for quantifying the sedimentation impacts.

The model simulations are benchmarked against variables such as discharge, sediment load, reservoir levels, and evapotranspiration. These data are obtained from local observations as well as through remote sensing.

The results show that improvements have been made to the models in terms of reservoir representation and the quantification of the evapotranspiration flux, which leads to small improvements in the discharge estimates for the Rhine and Danube. The ability of the water system models to better capture important processes like evapotranspiration and the reservoir storage is also hypothesized to positively reflect on their ability to capture the impact of future climate change and the human-water interactions.

In the Jucar case study basin, we find that coupling a hydro-economic model with a hydrological model can accurately estimate irrigation shifts in several regions in the Jucar basin as well predict the remaining discharge to the sea.

The impact assessment for the Mekong shows that by coupling hydrological model, reservoir expansion scenarios and the D-CASCADE model, sediment loads of the river can be decreased by 27 to 43%. The construction of dams will trap sediment which in turn will have an impact on the floodplain and delta development that in part depend on this sediment transport from upstream regions.

Regarding the impact models, we find interesting spatial patterns when it comes to the distribution and suitability of fish species to survive in different parts of the case study basins. For the Danube, we simulated the habitat suitability for 58 species, while for the Jucar (35), Rhine (25) and Mekong (27) the numbers of modelled fish species included in the ecosystem modelling was slightly lower. For the Mekong this is mostly the result of reduced data quality, while the known abundance of species in these regions is very high.

In conclusion, this deliverable describes how linkages are established between the water system models and the impact models. It includes the adjustments of existing model structures and shows how data from water models can be used to assess the ecological impacts of hydrological behavior.

Table of Contents

Publishable Executive Summary ***3***

Description of deliverable ***7***

Introduction ***7***

Methodology ***9***

Case Study Region and Associated Models **9**

Danube and CWATM 9

Jucar and its hydroeconomic model 11

Mekong 14

Rhine and PCRGLOBWB 2 19

Impact Models **21**

Biodiversity Models 21

Sediment Connectivity in the Mekong 22

Integration of modelling components **24**

Integration with biodiversity models 24

Integration with Sediment Transfer 25

Validation Datasets/Observational Data **27**

Danube 27

Jucar 30

Mekong 31

Rhine 33

Results ***34***

Danube **34**

Discharge 34

Reservoir storage 35

Evapotranspiration 36

Jucar **37**

Reservoirs 37

Streamflows 39

Deliveries 42

Albufera water balance 43

Mekong **45**

Rhine **51**

Biodiversity Modelling: Initial model predictions **57**

Examples of habitat suitability predictions for the Danube basin 57

Examples of habitat suitability predictions for the Júcar basin 58

Examples of habitat suitability predictions for the Rhine basin 60
Examples of habitat suitability predictions for the Mekong basin 62
Conclusions 63
References 65
Disclaimer 69
Acknowledgement of funding 69
Annex I: Table of figures 70

Description of deliverable

In this deliverable, we describe the integration of hydrological and impact models. These models are integrated to provide relevant information on the hydrological state for each of the case study regions. The impact models can translate the hydrological state and change therein into impacts on biodiversity, sediments and the economy. This powerful combination can inform us if there is sufficient water for water use sectors and if that water is also sufficient to sustain the natural ecosystem for the case study regions. This also serves as the benchmark for assessments of the biodiversity and water availability under climate change. Finally, the models are benchmarked against observational data to quantify the uncertainty on these model simulations. For this case study region specific information will be used when available.

Introduction

To study the impact of changing climate regimes and anthropogenic water use on current and projected water availability, researchers use hydrological models. These models typically require input of hydroclimatic variables such as precipitation, evaporation and temperature, to generate timeseries of discharge, reservoir levels and groundwater levels. In order to simulate current and projected water availability, these models should also have a detailed representation of the human-water interactions (e.g., reservoirs, irrigation and abstractions) (Hanasaki et al., 2008, Terink et al., 2015, Burek et al., 2020, Sutanudjaja et al., 2018, Schmied et al., 2023). Some state-of-the-art global hydrological models contain information about anthropogenic water use and human-water interactions (e.g., PCRGLOBWB2.0, CWATM, WaterGAP) that can then be used to better understand the current and projected impacts on water availability for different uses (Wada et al., 2014, Hanasaki et al., 2008, Schmied et al., 2023, Biemens et al., 2011, Sutanudjaja et al., 2018). In many cases, these models were previously limited by computational demand and the limited spatial resolutions of some of the required input datasets (30 arc minutes to 5 arc minutes). Recent advancements have made significant improvements in the parallelization of these models as well as downscaling the required input datasets, allowing them to operate at higher resolutions (30 arc seconds, Hoch et al., 2023, van Jaarsveld et al., 2024).

While global hydrological models are useful for evaluating a variety of hydrological indicators (e.g., discharge, reservoir storage, evaporation, water demand to name a few), in many cases they lack region-specific information regarding biodiversity, sediment transfer, saltwater intrusion, and detailed human water dynamics such as interbasin transfers. This regional information can be better represented by impact models that can model the small-scale interactions that lead to changes in these regional dynamics. In the cases where the regional dynamics are vital to the broader research objective, it may be useful to couple (by directly linking the outputs of the hydrological model to the impact model inputs) hydrological models to region specific impacts models that contain this information. This allows researchers to develop modelling frameworks that can be tailed to specific regional dynamics and stakeholder questions. These linkages also allow more detailed predictions regarding specific socioeconomic and biodiversity related impacts as well as yield insights into regional teleconnections.

Evaluating the direct impacts of both the individual models (either hydrological or impact models) as well as the coupling of the two is key to ensuring model results are accurate. To do this, modelers use

a variety of benchmarking datasets (for the purposes of this report, benchmarking refers to the combined validation and calibration). It is essential to first benchmark the individual water system models and their components before benchmarking the coupled scenarios, so a better understanding of individual model biases and performances can be acquired, and the linkages can be fully assessed. A variety of hydrologic, socioeconomic or biodiversity datasets can be used for this as long as the modelled outputs can be directly compared to the observation data (e.g. discharge cannot be validated against water extractions). For the combined systems, it can be useful to solicit the expertise of local stakeholders to ensure the model results are accurate to their systems and needs.

Within the SOS-Water Project, we aim to better evaluate the amount of water that can be allocated to different water use sectors under a variety of climate scenarios (better defined as a safe operating space). To evaluate this, our main goal is to develop an integrated water modelling system (IWMS) that can be used in the four case study basins (the Rhine, the Danube, the Mekong and the Jucar) to support model predictions across social, environmental, economic and hydrological variables. In our case, we have opted to link our global hydrological models to regional impact models that focus on key stakeholder concerns. To do this, we must first update our hydrological models with state of the art data in terms of spatial resolution, reservoir representation, climatic variables, and ensure we have accurate representations for all case studies. We then work to couple the hydrological models with the basin-relevant impact models to address the necessary stakeholder concerns. Finally, we validate and benchmark this IWMS in each case study to ensure that we can use it to inform stakeholders on potential water management policy recommendations.

In this framework we opted to use two global hydrological models that are globally available, but lack local inputs and two more regionally tuned models. The advantage of the regional model is that stakeholders are very familiar with their usage and quality, while the global models can be used fulfill any missing global interconnections and variables. In the cases where we only use global hydrological models, we have tailored these models to use more local inputs on management and parameterization and thus act more as a local model for those specific catchments. In the situations where we have global and local models we can compare the difference between the different models. By testing the framework with a diversity of models in a diversity of regions, we can evaluate the robustness of the proposed methodology and ensure it connects to the stakeholder needs. By using multiple model we can also quantify the model uncertainty, however the ensemble size is still limited compared to some of the large Multi-Model MIP experiments (which are typically run by very large consortia). Nonetheless we aim to have an uncertainty quantification by having a minimum of two hydrological models per region, five climate models and three socio-economic scenarios, we can still provide a total 30 ensemble member and help to quantify the uncertainty of our projections. The uncertainty in meteorological forcing can be addressed by the use of a variety of forcing datasets that allow for quantification of the uncertainties in model response to changing meteorological conditions. At the same time by using multiple models we can identify if adaptions strategies show a robust response across a variety of global and local models. This provides additional insight on the robustness of this project's findings and valuable information to the stakeholders involved.

Over the past two years of this project, we have developed this IWMS (defined as a combined modelling system focused on hydrologic impacts) and in this report, we will describe the current modelling system for each of the four case study regions in the SOS-Water Project as well as the

benchmarking results. We will describe the potential impacts of this system both for the SOS-Water Project but also to other projects and researchers.

Methodology

Case Study Region and Associated Models

Danube and CWATM

The Danube Basin includes 19 countries, is home to 79 million people and covers an area of 801,000 km2, which makes it the second largest basin in Europe and the 21st largest in the world. The Danube stretches over 2,850 km from the Black Forest (Germany) and flows south-eastward through Europe to the shores of the Black Sea.

Due to its extent, variety of habitats, flowing conditions, and diversity of characteristics, the Danube Basin is conventionally divided into upper, middle, and lower sections (Figure 1). The upper basin extends from the source, in the German Black Forest, to the capital city of Slovakia, Bratislava. The middle basin stretches from the Gate of Devin Castle, near Bratislava, to the Iron Gate Gorge, at the border between Serbia and Romania. The lower basin begins downstream of the Iron Gates. From there, the Danube meanders across a vast plain, spreading out and becoming shallower and marking a natural border between Romania and Bulgaria. The course of the Danube ends and opens into the Danube Delta, formed by the river splitting into three channels named Chilla, Sulina, and Sfintu Gheorghe (St. George), caring for approximately 63%, 16%, and 21% of the discharge, respectively. The delta is the largest in Europe, covering an area of approximately 6,000 km².

The hydrological regime of the upper and part of the middle basin, down to the confluence with the Morava River, is glacio-nival, with peak discharges in July and lows in winter (January-February). While the influence of the glacial regime persists to the mouth of the Tisza River, the discharge pattern changes further downstream where the influence of larger tributaries like the Tisza and Sava Rivers lead to a bimodal discharge regime similar to the lower Sava and Drina Rivers. This bimodal regime features two annual peak discharges and low flows occurring in late autumn and spring (high flows) and winter and summer (low flows), respectively.

The Danube River Basin serves as a vital resource for various economic sectors, including energy production, agriculture, and industrial activities. However, the cumulative pressure exerted by these diverse water uses poses significant challenges to the basin's water system. The ecological and chemical status of surface waters within the basin is threatened by factors such as organic pollution, nutrient loading, hazardous substances, and hydromorphological alterations. Moreover, impacts of climate change such as drought, water scarcity, and extreme hydrological events, will likely exacerbate these negative pressures if left unmitigated.

Figure 1: Depicts the basin boundaries of the Danube River Basin. The Danube River is shown in blue, while the upper basin is outlined in black. The middle basin is outlined in purple and the delta in navy.

CWatM is a grid-based global hydrological model developed by the International Institute for Applied Systems Analysis (IIASA) (Burek et al., 2020). It is designed to simulate the water cycle on a daily time step considering factors like precipitation, evaporation, runoff, groundwater flow, and human water use. CWatM can be applied at both global and regional levels, allowing for analysis of water issues in different contexts and to simulate future water availability and demand under different scenarios.

The components of the hydrological cycle and the water management processes simulated by CWatM are displayed in Figure 2 and can be classified into the following five categories:

1. Runoff components, including the surface runoff, interflow, interception, soil infiltration and percolation, soil properties;
2. Routing component is made by kinematic wave approach, considering the physical characteristics of the river channels, such as slope, cross-sectional area, and roughness;
3. Groundwater components include the linear storage reservoir;
4. Meteorological model, which includes the snow water model, evapotranspiration and forcing data such as air temperature and precipitation;
5. Water management components, including reservoir management, water demand for different economic sectors and domestic usage;

In addition to these components which are part of the standard implementation, CWatM was enhanced with the integration of the Open Global Glacial Model (OGGM) and open-source glacier model (https://oggm.org/) designed to simulate the past and future evolution of glaciers. Further enhancements encompassed the development of a detailed dataset of crop specific irrigated areas and dam operations schemas.

Further enhancement was the replacement of three key simplifications of the reservoir operations routine. First, static storage thresholds were replaced with seasonally varying operating coefficients derived from observed filling patterns; second, generic outflow rules were replaced with Ratio-Release curves providing daily release ratios from observed storage-discharge relationships; and third, rectangular geometry assumptions were replaced with Volume-Elevation-Area relationships from satellite-derived bathymetry. These innovations collectively improve the representation of temporally variable operations and physically consistent storage dynamics.

An overview of the data needed, and data structure of CWatM is given in Burek et al. 2020 or https://cwatm.iiasa.ac.at. A detailed description of the components and processes is available at https://cwatm.iiasa.ac.at/modeldesign.html. CWatM is open source, and a description of the processes, the variables and the source code is given at https://cwatm.iiasa.ac.at/sourcecode.html. The source code of the different components is stored and further developed on: https://github.com/iiasa/CWatM.

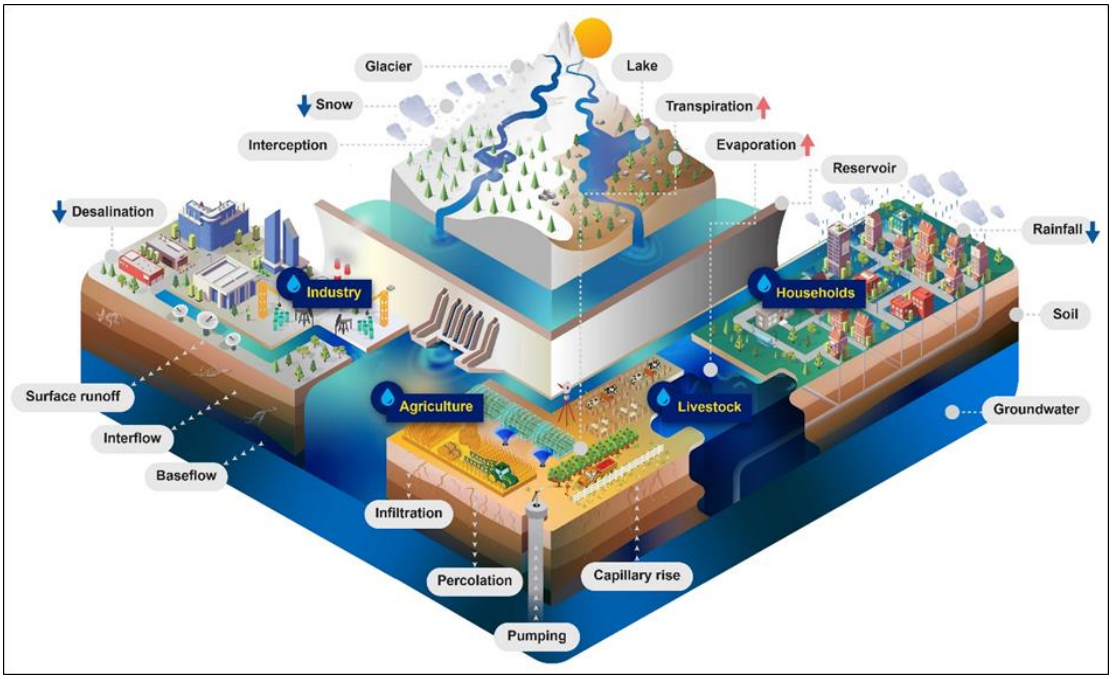

Figure 2: Components of the hydrological cycle and the water management process simulated in CWatM

Jucar and its hydroeconomic model

With an area of 22,261 Km^2, the Jucar River Basin (JRB) is one of the most important rivers in Eastern Spain. Its main tributaries are the Cabriel, Magro and Albaida rivers (Figure 3). Its climate is mostly semiarid, with annual precipitations ranging between 300 and 820 mm with a Mediterranean pattern, combining Autumn heavy rainfall events (and thus flood risk) with dry summers. Its mean total annual

surface runoff is equal to 1,456 Mm^3/year (1940-2018 period, decreasing to 1,245 if the period 1990-2018 is considered), following the same pattern as rainfall does (CHJ,2023). Its hydrological basin can be divided between upper basin (upstream of the Alarcon and Contreras reservoirs), middle basin (between those reservoirs and the downstream Tous reservoir) and lower basin (downstream of Tous). The middle basin includes the most relevant groundwater body of the Jucar river basin, the Mancha Oriental aquifer, whose stream-aquifer interaction dominates the Jucar River runoff in its middle streams. Although formerly a semi-endorheic zone (connected to the Jucar exclusively through groundwater discharge), the Mancha Oriental plain was connected to the Jucar by the Maria Cristina canal in the 19th century. In the basin, there are also two endorheic zones with no direct surface connection with the Jucar River: one north of its mouth, which drains to l'Albufera wetland, and one in the south whose discharge is collected at the Almansa reservoir and serves local farmers. The first endorheic zone receives water from the Jucar in an indirect way through the surface, and groundwater returns from the neighboring agricultural demands.

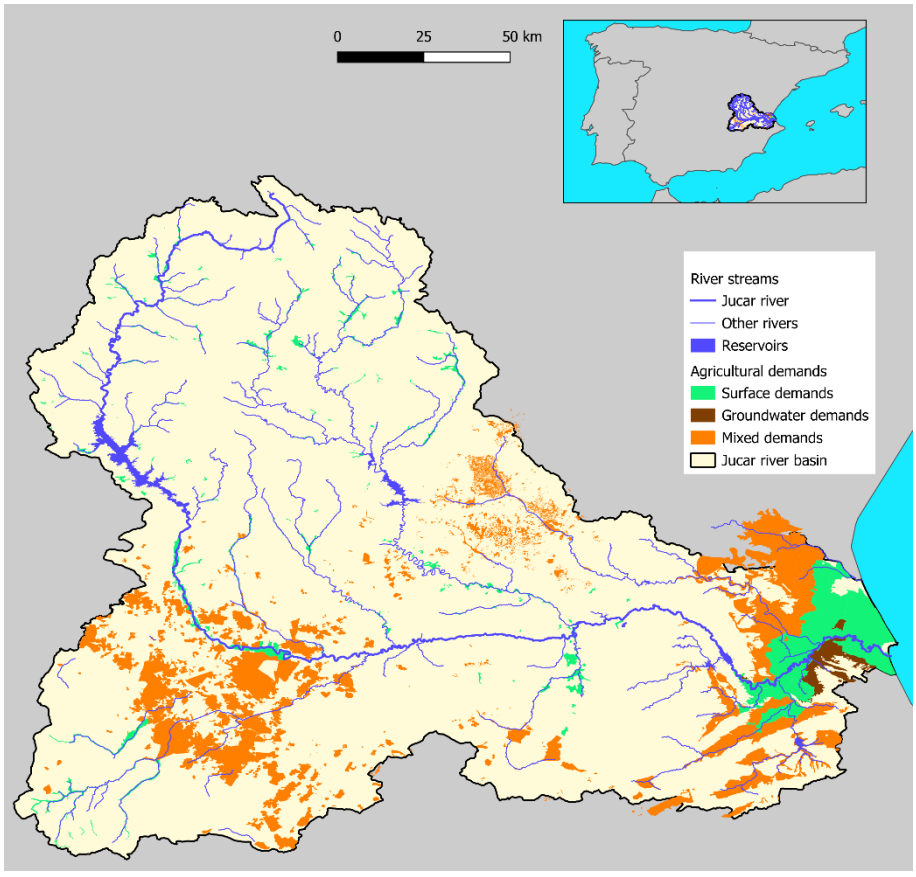

Figure 3: Jucar river basin location map

The annual demand is equal to 1,486 Mm^3/year, with the principal uses for water being agricultural use (89%), followed by urban (9%) and industrial uses. The fact that demands are higher than surface resources, in addition to the existence of drought periods, requires careful water planning and management combined with distinct infrastructure developments. In this regard, the Jucar has 11 reservoirs with more than 1 Mm^3 of capacity, being the most important the Alarcon (1,118 Mm^3 of capacity), Contreras (around 450 Mm^3 of real capacity) and Tous (379 Mm^3 capacity but subject to provide empty storage for flood protection) reservoirs. Furthermore, there are three hydropower

reservoirs in the downstream part of the middle basin of the Jucar (Molinar, Cortes II, Naranjero), although their role in river regulation is minimum. Moreover, the Jucar River system has three main canals devoted to conveying surface resources for urban and irrigation demands (Acequia Real, Jucar-Turia and Tagus-Segura). Although the main purpose of the Tagus-Segura canal is to convey water between the Tagus and the Segura basins, the Jucar River basin is allowed to use it to transport water from the Alarcon reservoir to the Mancha Oriental area.

The hydro-economic model of the Jucar river basin has been developed using the Explicit Stochastic Programming Advanced Tool (ESPAT) developed by Macian-Sorribes et al. (2017). This model employs a simulation approach that reproduces the current water resource management in the Jucar River system at the monthly scale. It conceptualizes the river using 27 nodes, 8 surface reservoirs, 5 groundwater bodies modelled using the Embedded Multi-reservoir Model (Pulido-Velazquez et al., 2005), 7 sub-basins, 18 consumptive demands, 9 hydropower plants and 6 minimum environmental flows (as described in the hydrological plan). The representation of the system for this model is presented in the next figure.

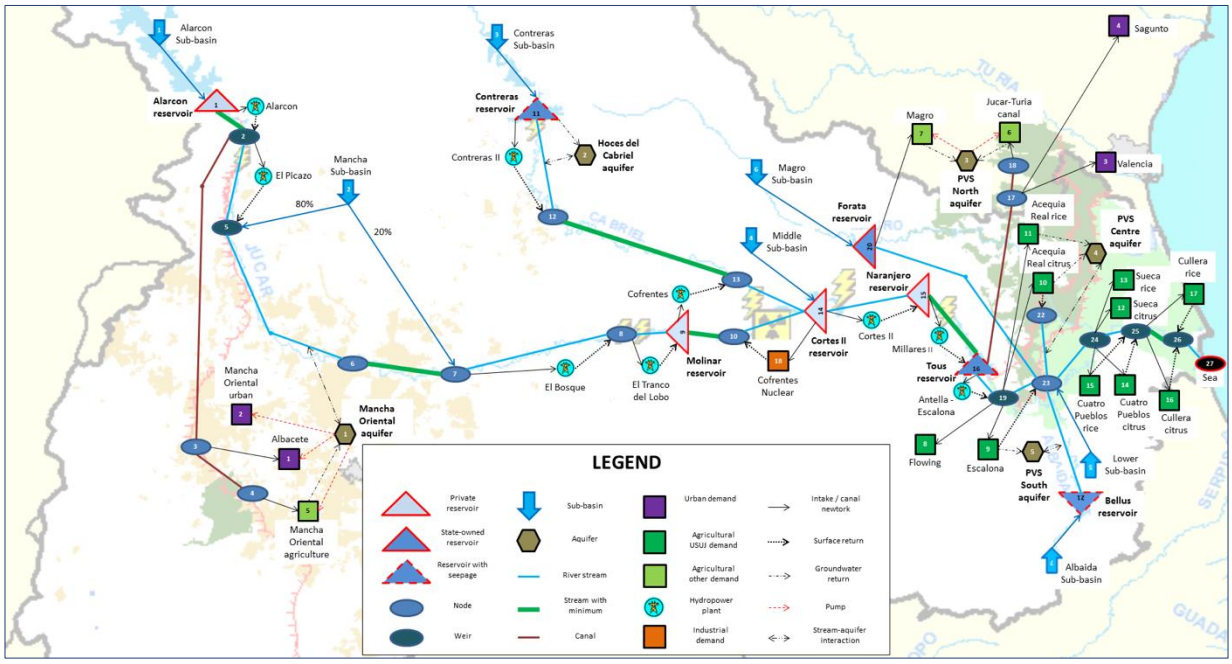

Figure 4: Schematic of the Jucar river hydro-economic model

The model's physical attributes - hydrological sub-basins, reservoir features (capacity, minimum level, storage-head, and storage-surface curves), groundwater dynamics, river reach and canal capacities, prescribed minimum streamflow, water demands, return flows, and fish habitat details - were gathered from the Jucar River Basin Agency. Economic aspects related to water usage, like urban water needs, energy prices, and pumping expenses, were first taken from the Jucar River Basin Management Plan (CHJ, 2023) and past studies (Pulido-Velázquez et al., 2006) within the DMA rollout in the Jucar, part of the EU AQUAMONEY project. These economic factors were compared with other Jucar models (Kahil et al., 2016) with adequate results. Urban water demand was characterized using demand functions that establish a connection between water supply levels and the marginal utility of water for consumers. On the other hand, agricultural water demand linked to citrus, orchards, and perennial

crops was modelled through an adapted approach to crop yield calculations derived from FAO66 methodologies (FAO, 2012). This method calculates yearly crop yields based on monthly supply-demand ratios, then estimates total food production from this yield and they compute total benefits based on crop prices. Crop yields and prices were obtained from the annual statistics published by the Ministry for Agriculture, Fishery and Food of Spain. Rice cultivation significantly contributes to maintaining l'Albufera Lake, a vital protected area in the region, and its water supply has been treated as a constraint. The only industrial water demand from surface water comes from the Cofrentes Nuclear Power Plant. Its benefits per unit of water consumption were assessed employing the alternative cost approach, which factors in the cost of generating equivalent energy via gas minus the operational expenses of the plant, as detailed in Pereira-Cardenal et al. (2014).

Mekong

The Mekong River spans nearly 4,800 km, with a drainage area of 795,000 km². Originating in Tibetan plateau, the Mekong flows through six countries: China, Myanmar, Laos, Thailand, Cambodia, and Vietnam, ultimately forming one of the world's largest deltas before emptying into the East Sea. The basin is divided into three regions: the Upper Mekong (China and Myanmar), the Lower Mekong (Laos, Thailand, Cambodia, and Vietnam), and the Mekong Delta (Cambodia and southern Vietnam) (Figure 5). The river's average annual flow is around 475 km³, with the majority (82%) originating in the Lower Mekong, while the Upper Mekong accounts for only 18% of the yearly flow. This Upper portion, however, plays a crucial role during the dry season, contributing about 30% of the total flow. The Mekong is the second most biodiverse river in the world, after the Amazon, and supports the largest freshwater fishing industry globally, with an annual catch of approximately 2.3 million tons. The river basin lies in a tropical climate zone characterized by high humidity and abundant rainfall. Rain, the primary water source, averages about 1,600 mm annually across the entire basin. The rainy season, which spans from May to November, typically begins earlier in the upstream reaches and ends later downstream. The peak rainy period from May to October defines the wet season, while November to April marks the dry season. Given the necessity of modeling different parts of the Mekong River system with distinct approaches, we divide the Mekong system into two regions: the Upper Basin (Upper and Lower Mekong) and the Mekong Delta, each with its own characteristics, criticalities, and tailored models.

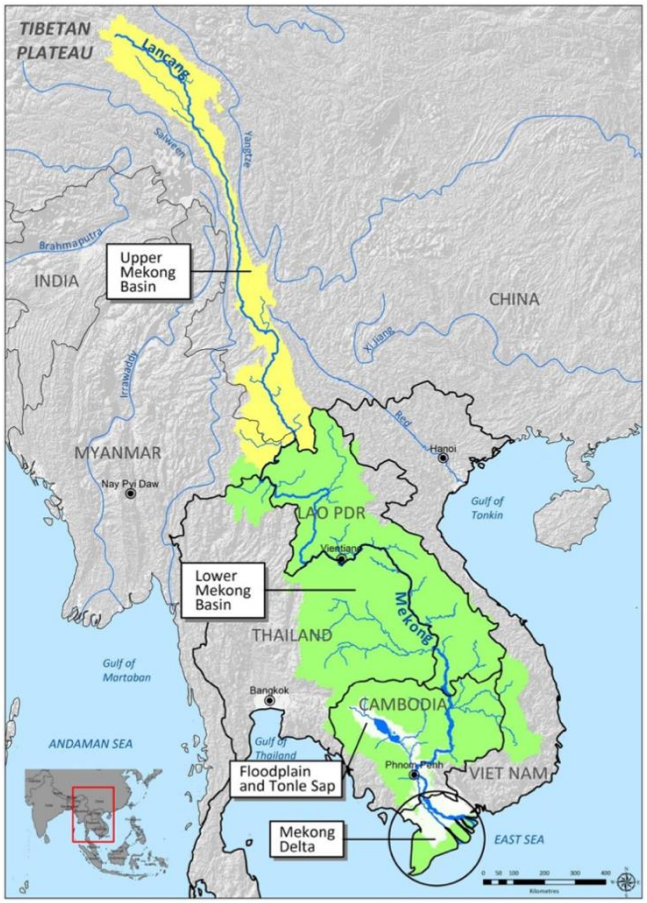

Figure 5: Mekong River basin location map

Upper Basin, Vic-Res and D-CASCADE

Historically, the development of water infrastructure in the Upper Basin has been carried out without a comprehensive perspective on the benefits and impacts of these projects on the entire Mekong River system, leading to a series of critical issues for the societies and ecosystems that depend on the Mekong. Since the 1960s, over 160 large dams have been constructed on the Mekong River and its tributaries, with hundreds more either planned or under construction (Ang et al., 2024). While hydropower development aims to promote sustainable economic and social progress by generating valuable energy, it has significantly altered the river's natural dynamics. These dams disrupt the flow of sediment and nutrients, block migratory routes for aquatic species, fragment river ecosystems, and cause significant changes in seasonal flow distribution (Ziv et al., 2012, Poff et al., 2007). These changes have profound impacts, particularly downstream and in the Mekong Delta, where both ecosystems and human societies depend heavily on the river's resources. The reduced sediment flow worsens delta subsidence (Kondolf et al., 2022), while the disruption of fish migration threatens the sustainability of the region's large freshwater fishing industry (Ziv et al., 2012).

The hydrological dynamics of the upper Mekong basin are modeled using VIC-Res, a large-scale hydrological-water management model (Dang et al., 2020). VIC-Res operates through a two-step modeling approach. The first step uses the Variable Infiltration Capacity (VIC) model, a semi-distributed hydrological model that accounts for both water and energy balances on a large scale (Liang et al.,

1994). In this step, each grid cell is divided into one vegetation layer and two or three soil layers, for which the model calculates evapotranspiration, infiltration, runoff, and baseflow on a daily time step.

The runoff generated in each VIC cell is then independently processed by VIC-Res, which simulates streamflow routing. VIC-Res collects gridded surface runoff and baseflow data from VIC to model river discharges throughout the river network, also on a daily time step. The routing process relies on a flow direction matrix and a linearized version of the Saint-Venant equations.

Moreover, VIC-Res has the ability to represent water reservoirs and their operations within the routing model. Each reservoir is modeled with a cell representing the dam location and multiple cells representing the water body, where the mass balance is computed. Release decisions are based on predetermined rule curves that account for water availability, incoming inflow, and dam design specifications. Using this information, along with data on hydraulic head and releases, VIC-Res calculates the daily amount of electricity generated and the river discharges along the network (Figure 6).

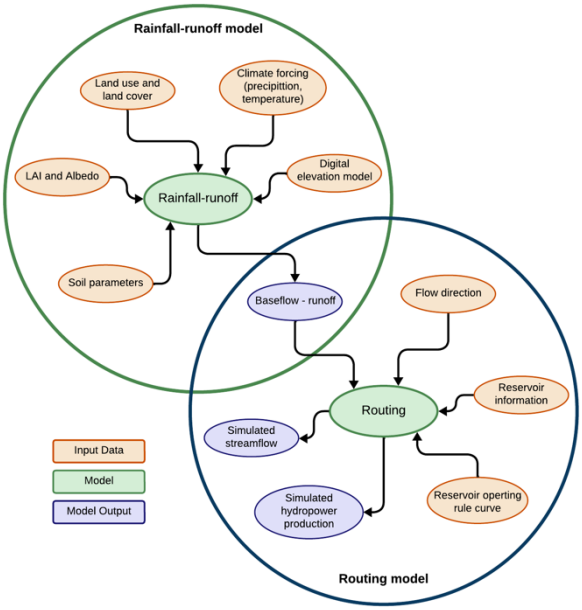

Figure 6: Schematic showing the coupling between Vic-Res using the combined rainfall-runoff model and the routing model.

The model implementation has a spatial domain of ~630,000 km^2, stretching from the upper reaches of the Lancang in China to the gauging station of Stung Treng in Central Cambodia. Overall, we account for a total of 129 dams, each having storage capacity or installed capacity larger than 1 Mm^3 and 5 MW, respectively. The model has a spatial resolution of 0.0625 degrees, necessary to avoid allocating multiple dams to the same cell. The current setup and input data improve the version presented in Chowdhury et al. (2021) and Galelli et al. (2022) through the following updates: (1) the climate forcings (retrieved from CHIRPS and ERA 5) now span the period 1981-2022; (2) the bathymetry of each reservoir builds on detailed information retrieved from either the SRTM (v3) digital elevation model or a recently-released database of hypsometric curves (Hao et al., 2024)); (3) the operating rules of each reservoir are derived from time series of absolute reservoir storage estimated from Landsat images through the InfeRes python package (Mahto et al., 2024).

Mekong Delta and VRSAP

The Mekong Delta of Vietnam (MDV) is the most downstream part of the Mekong river basin, including 13 provinces/cities: Long An, Tien Giang, Dong Thap, Vinh Long, Tra Vinh, Hau Giang, Soc Trang, Ben Tre, An Giang, Kien Giang, Bac Lieu, Ca Mau and Can Tho, with the total natural area of about 3.96 million ha (not including the area of islands). This natural area accounts for 79% of the entire Delta, and 5% of the whole Mekong River Basin.

The Mekong Delta plays an important role in the socio-economic development strategy of the country. With a huge agricultural potential, the Mekong Delta in recent years has always contributed over 50% of the total national rice production, contributing to the national strategy for food security, and is a significant contribution in rice export (more than 90%). Besides rice, the Mekong Delta also provides about 70% of fruit production and over 75% of the total fishery production in the country.

However, although located in the lower Mekong River Basin, and with many inherited advantages (including geographical location, abundant water resources, natural regulation by the Tonle Sap Lake, large coastal region, open sea resources, flat land with fertile alluvial, and abundant, diversity fisheries), the Mekong Delta faces the impacts of natural conditions. These impacts range from the frequent and unpredictable effects from climate change, the upstream activities (e.g. pollution, water abstractions and reservoir management), sea level rise, saltwater intrusion, and above all, the conflict between economic growth and environmental protection issues in this Delta. In the process of socio-economic development in the Mekong Delta, the limitations of natural conditions and water related-risks (flood, drought, salinity intrusion, river bank erosion and land subsidence) are always barriers, especially for agricultural and domestic activities of people.

Due to the characteristics of the Mekong Delta region with low and flat terrain, tidal influence hydrological regime, dense network of canals, complex network of roads and dykes in flood areas, only hydrodynamics (1D or Coupling 1D & 2D) can give good simulation results of the flow in the Mekong Delta region. The most successful model applied to the Mekong Delta so far is the VRSAP model (VRSAP is the abbreviation of Vietnam River Systems And Plains) developed by SIWRP's experts (SIWRP, 2021, Hydraulic report for the Mekong delta). VRSAP is a program to calculate unsteady flows and salinity intrusion on the river and canal network, expanded to consider water exchange between rivers and floodplain in the delta, and including rainfall-runoff module.

The flood model includes the following hydraulic systems:

- The main Mekong River body from Kratie (Cambodia) to the sea;
- Tonle Sap Lake;
- Some important tributaries in Cambodia (Prek Dang Kom, Prek Ou Mal, Mul Kom Pul between the Mekong River and Tonle Sap, Tonle Toch, Stung Slot, Trabek on the left bank, Prek Thnot, Takeo, Chau Doc on the right bank, main canals and over 300 canals connecting the Mekong River, Bassac with the flooded area in Cambodia);
- Main surrounding river in Vietnam (Vam Co Dong, Vam Co Tay, Saigon rivers);
- All main canals and most key secondary canals in in Vietnam;
- The network of national and provincial highways, along with bridges and culverts on the system in the flooded areas of Vietnam and Cambodia;
- All floodplain in Vietnam and Cambodia with an area of up to 5.2 million hectares.
- The upstream boundary condition is the flow discharge at Kratie and some other river branches;

- The downstream boundary condition is the water level at the estuary hydrological stations (Vung Tau, Vam Kenh, Ben Trai, My Thanh, Ganh Hao, Xeo Ro and Rach Gia).
- The input rainfall is taken from the actual measurement data at 30 stations distributed in the territory of Vietnam and Cambodia.
- Topographic documents include digital elevation maps (DEM), designed and survey data of the structures (river and canal cross-section, road and dike elevation, culvert and dam dimensions, operation procedures of water work).

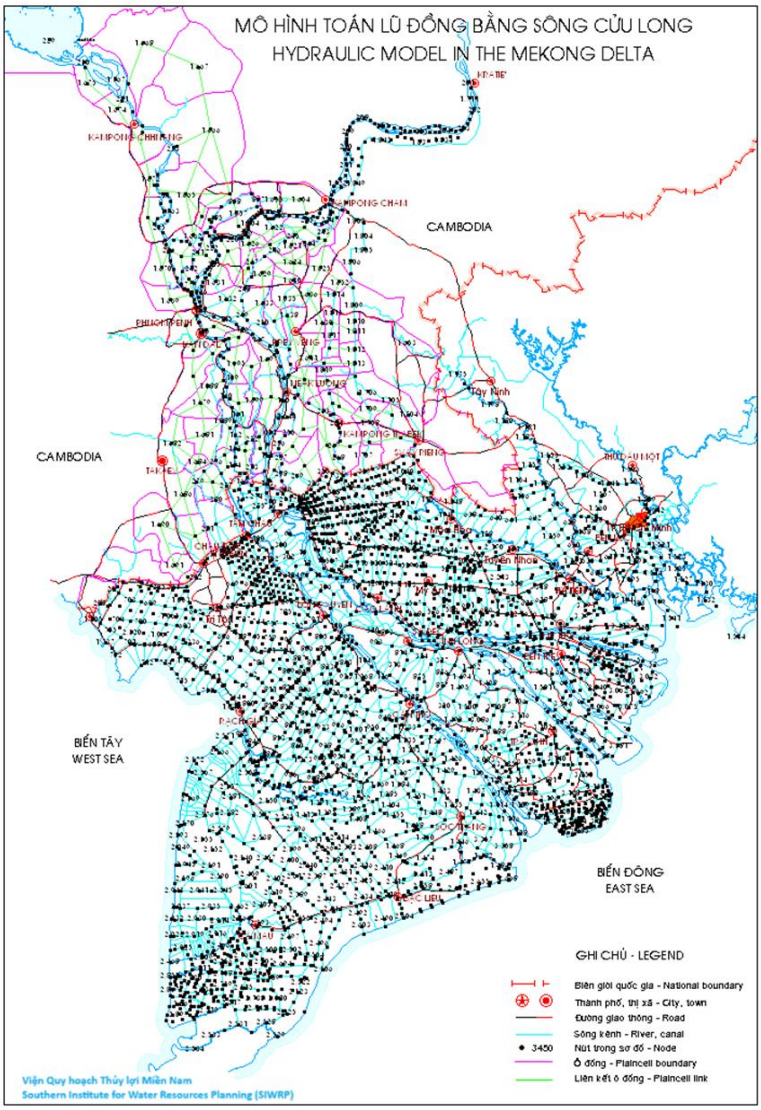

Figure 7: The figure shows VRSAP model network in the Mekong delta. Nodes are shown in black and the necessary linkages are shown in red, pink, green, and blue.

Rhine and PCRGLOBWB 2

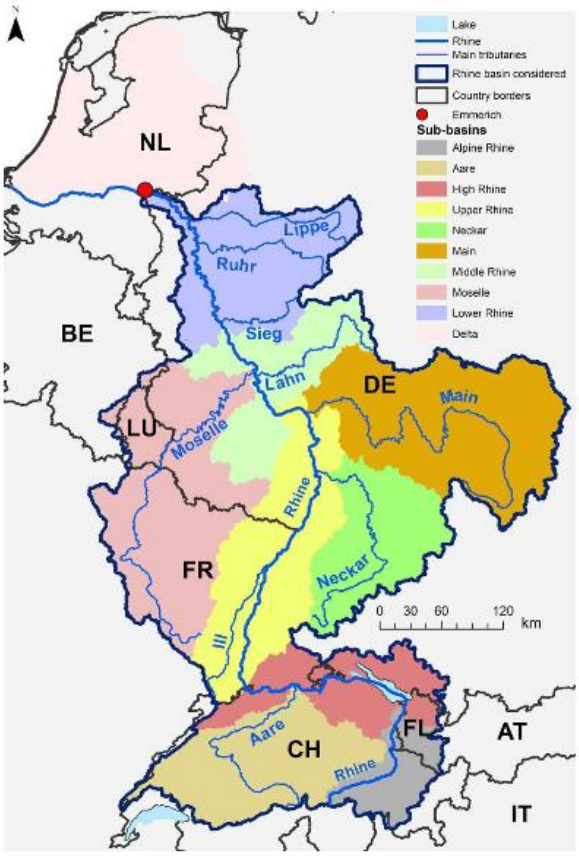

Figure 8: Map of the Rhine Catchment obtained from Moser et al (2018)

The Rhine River, spanning a length of approximately 1,230 km, is a major watercourse in Europe. It has a vast drainage area of around 185,000 km2, encompassing various sub-basins and tributaries (as shown in Figure 8). The source of the Rhine River is in the Swiss Alps in the canton of Graubünden, from which it flows through diverse landscapes, including mountainous regions, fertile valleys, and urbanized areas. The hydrology in the Rhine basin is dominated by groundwater driven flow, with longer residence times in the groundwater system. Together with its tributaries, the Rhine forms a diverse range of ecological habitats, including mountain streams, floodplains, wetlands, and estuaries, supporting a rich biodiversity in the region. Moreover, the Rhine plays a crucial role in maintaining ecological connectivity, allowing for the migration and dispersal of species. In addition to serving as an essential navigation route, facilitating trade and commerce within Europe, the Rhine River is also a significant source of water resources, providing drinking water, supporting industrial processes, and facilitating agriculture in the region. The Rhine has been studied extensively in many scientific publications and is focus regions for scientific peer-reviewed studies. Current issues we are addressing in the Rhine relate to low flows that inhibit navigation and transport, decreased river connectivity, increased water extractions and decreased water quality due to farming and shipping pollution. The models used for SOS-Water, PCR-GLOBWB_2, belong to the state-of-the-art hydrological models for this catchment and comparison between PCR-GLOBWB 2 and other models show that the model's

capability to capture the important baseflow component for Rhine simulations are good to excellent (Sutanudjaja et al., 2018).

PCR-GLOBWB 2 is a grid-based global hydrology and water resources model developed at Utrecht University (Sutanudjaja et al., 2018). The computational grid has a 5 arc-minute resolution (~10 km at the equator) and covers all continents except Greenland and Antarctica. Time steps for hydrology and water use are one-day, while the internal time stepping for hydrodynamic river routing is variable. For each grid cell and each time step, PCR-GLOBWB 2 simulates moisture storage as well as the water exchange between the soil, atmosphere and underlying groundwater reservoir. The exchange with the atmosphere comprises precipitation, evaporation from open water, snow and soils and plant transpiration, while the model also simulates snow accumulation, snowmelt, and glacier melt. PCR-GLOBWB 2 simulates runoff partitioned into surface runoff, interflow, and groundwater recharge as well as routing of water over the terrain. Runoff generated by snow and glacier melt, surface runoff, interflow, and groundwater is routed across the river network to the ocean or endorheic lakes and wetlands using the kinematic wave approximation. It is also possible to include floodplain inundation and to simulate surface-water temperature. PCR-GLOBWB 2 includes over 6000 manmade reservoirs from the GRanD database that are progressively introduced in time and a reservoir operation scheme dependent on each reservoir's purpose. Human water use is fully integrated with the hydrological model. Thus, at each time step: 1) water demand is estimated for irrigation, livestock, industry, and households; 2) these demands are translated into actual withdrawals from groundwater and surface water (rivers, lakes, and reservoirs) subject to availability of these resources and maximum groundwater pumping capacity in place; and 3) consumptive water use and return flows are calculated per sector (Figure 9).

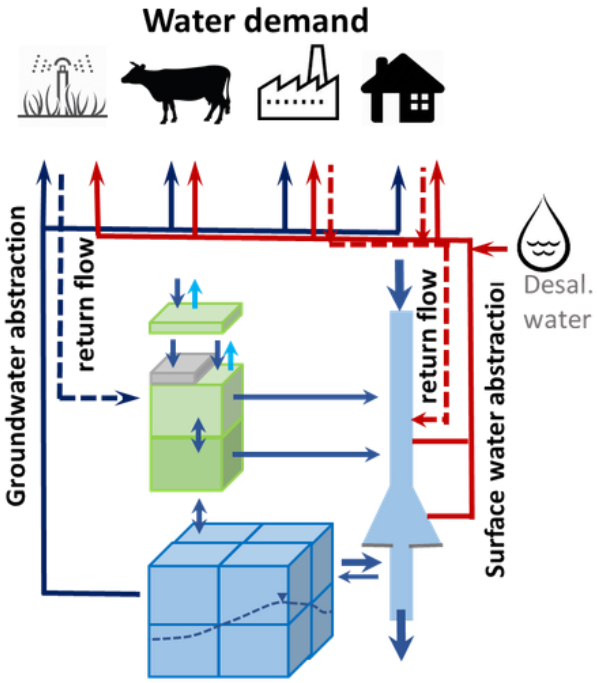

Figure 9: Schematic drawing of a the human water use components in PCRGLOBWB 2 from Wada et al., 2014.

Currently, the PCR-GLOBWB 2 model uses a generic reservoir scheme that uses reservoir inflow, long term average outflow and reservoir maximum capacity to determine releases at every time step. This scheme, implemented in PCR-GLOBWB 2 by Van Beek et al., 2011, allows for releases to be determined using very limited data requirements. Within the SOS Water project, we wanted to expand upon machine learning methodologies and the increase in remotely sensed reservoir datasets to 1) update the number of reservoirs in PCR-GLOBWB 2.0 and 2) update the reservoir operations from a generic operation scheme to a data derived one using remotely sensed data from GloLakes Hou et al., 2024 and operational bounds from STARFIT Turner et al., 2021. Therefore, in our validation section, we primarily focus on the validation of these updated operational policies and changes.

Impact Models

Biodiversity Models

To model freshwater biodiversity for all case studies, the methodologies used for species distribution modelling were applied. Species distribution models (SDMs) are broadly defined as spatial statistical models which provide a powerful tool to combine spatially explicit biodiversity information, i.e. species geographic occurrence data, with a suite of environmental information that is deemed important for describing the spatial distribution of the habitat suitability of species (Elith et al. 2009) (Figure 10). While such models can be primarily used to assess the current, or present-day potential distribution of a given species, it is also possible to first train the model with the present-day data but to then project the model into geographic space using scenario data. In this regard, SDMs allow researchers to assess the relative contribution of a specific environmental variable (i.e., spatial layer) on species' habitat suitability, and allow addressing the magnitude of change of an environmental layer (e.g., mean annual discharge) and its effect on the habitat suitability maps.

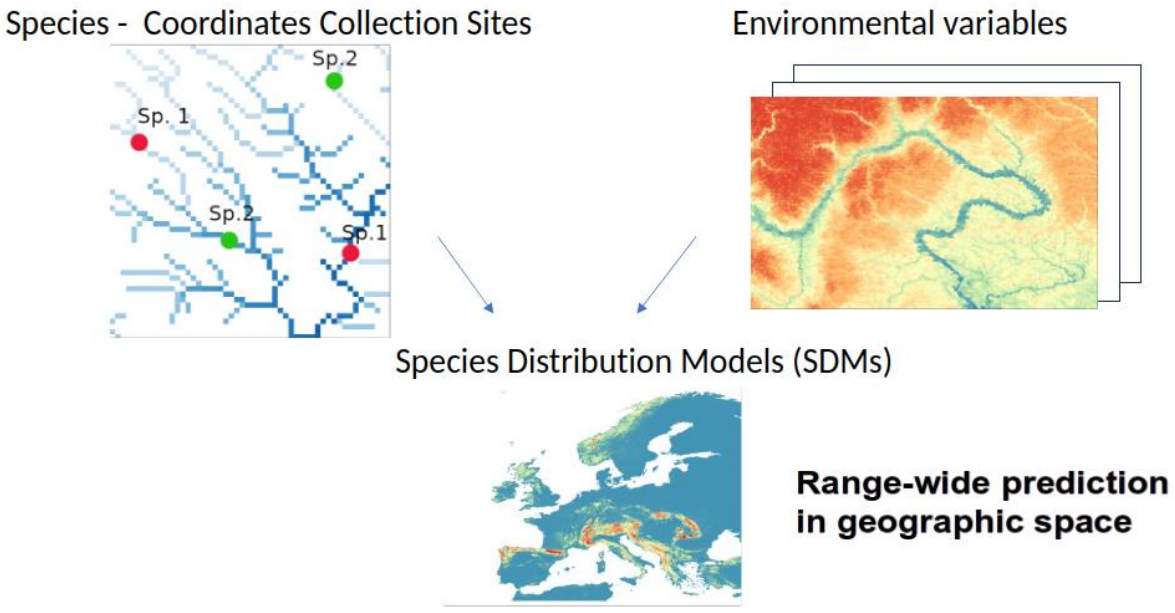

Figure 10: Workflow of Species Distribution Models. The location records of a species are overlain with a series of previously selected environmental layers known to characterise the species' habitat. This involves the determination of the mathematical

In SOS-Water, SDMs are applied across all case studies following a standardized methodology using fish as indicator species, such that the methodology would also allow comparisons among the case studies if needed. While the distribution modelling is ongoing, the entire modelling workflow for each case study has been developed and initially tested with stream topographic, climatic, land cover, soil and discharge variables.

Biological data

The biological data consists mainly of fish occurrence information. The collated databases for all case studies provide information on the location where fish individuals were observed or collected or literature registers. This location is represented by geographical coordinates. In addition, information is also available regarding the date of collection, but this information is not available for all records.

The compilation of the biological data for all case studies has been done by retrieving the information from the following public repositories:

- the Global Biodiversity Information Facility (GBIF) (https://www.gbif.org/)
- Fishnet (http://www.fishnet2.net)
- idigbio (https://www.idigbio.org/)
- vernet (http://www.vertnet.org/)

For the Jucar case study, the publicly available information has been integrated with biological information provided by the UPV partners who had access to local databases.

Environmental data

The models primarily used environmental data from the *Environment90m* dataset (Garcia Marquez et al., in prep). This dataset aggregates topographical, climate, soils and land-cover information for all subcatchments delineated in the Hydrography90m dataset (Amatulli et al. 2022). Specifically, summary statistics (i.e., mean, standard deviation, minimum, maximum and range) across all sub-catchments were calculated for a total of 106 environmental variables, including 47 variables related to topography and hydrography, 19 climate variables (current and future), 22 land cover categories (the proportion of each land cover category was calculated per subcatchment) and 16 soil variables.

In addition, the models capitalized on the discharge data available for Europe as produced by the PCR-GLOBWB 2 (Sutanudjaja et al., 2018). Water discharge was also aggregated to the identical sub-catchments as the other environmental variables.

Sediment Connectivity in the Mekong

In the upper portions of the Mekong River basin (denoted as the Upper and Lower Mekong without the delta), sediment connectivity is modeled using a dynamic, one-dimensional network-based sediment connectivity model called D-CASCADE. D-CASCADE conceptualizes sediment transport as a series of individual 'cascades' and tracks the positions and movements of sediment over time and space, allowing for the exploration of sediment supply and delivery patterns across the basin (Tangi et al., 2022). The model represents the river system in one dimension, mapping the river network as a directed graph of nodes and reaches, each characterized by specific hydromorphological attributes.

D-CASCADE calculates the daily transport capacity of each reach using the Engelund & Hansen Transport Capacity formula (Engelund & Hansen, 1967) and simulates sediment transport as cascades that originate from upstream sources. Additionally, the model accounts for the presence of hydropower reservoirs along the river network and their impact on sediment transport. For each reservoir, it calculates the daily Trap Efficiency, considering the Brune Curve (Gill, 1979) and the grain size of the sediment class involved. The amount of mobilized and transported sediment is then reduced by the computed Trap Efficiency, reflecting the sediment trapping effect of the reservoirs (Figure 11).

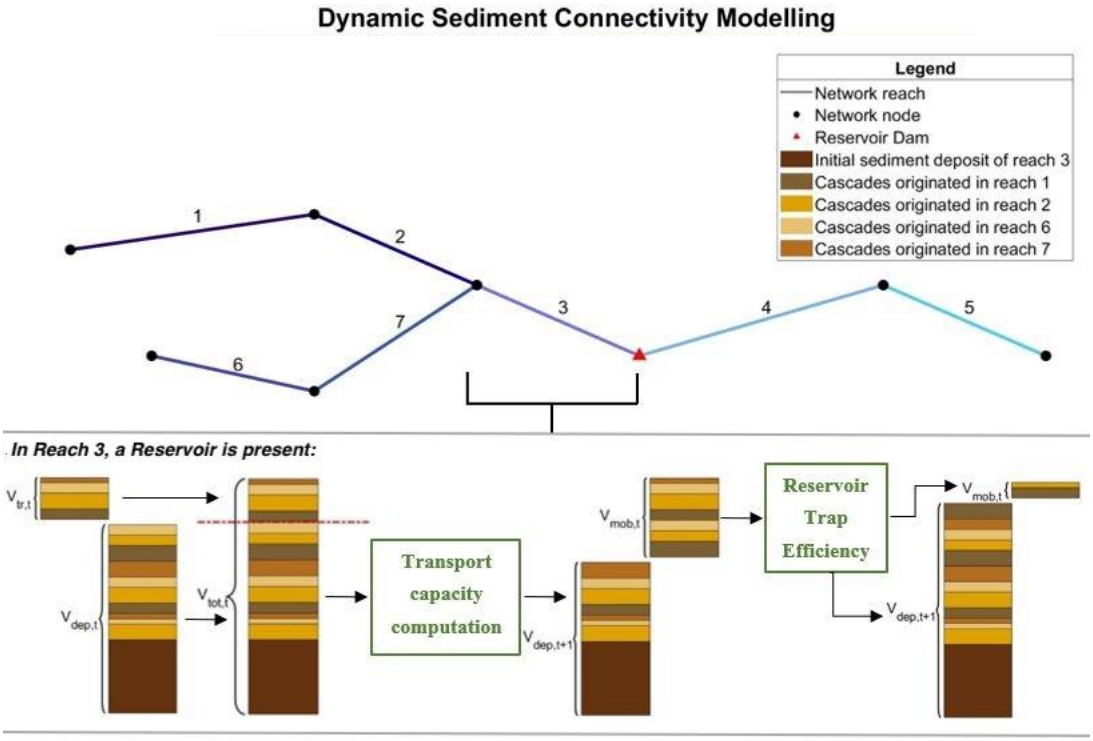

Figure 11: Schematic overview of the D-CASCADE model from Tiang et al., 2022.

D-CASCADE Mekong is built on the same spatial domain as VIC-Res Mekong, covering the area from the upper Mekong River basin in the Tibetan Plateau to Stung Treng in Cambodia, allowing for the integration between the two models. The extracted river network spans 4,257 km, comprising 854 reaches with an average length of 32.6 km each. Additionally, the model includes the 129 reservoirs also represented in VIC-Res, assigning them to their respective reaches within the river network.

MIKE 11 is a specialized water engineering software for simulating water levels, water flow, water quality and sediment transport in river mouths, channel systems and other water storages. MIKE 11 is a user-friendly, one-dimensional dynamic modelling tool for detailed analysis, design, management and operation of complex rivers and channel systems. With its exceptional user-friendliness, flexibility and speed, MIKE 11 provides an effective design environment for engineering, water resources, water quality management and planning applications. In the Delta, i.e. from Kratie and downstream at least two other well proven and detailed quasi 2-D model are maintained by SIWRR and SIWRP, respectively. These models, which are both based on MIKE11 technology, are quite detailed and have previously been used for sediment and erosion studies. Furthermore, the Mike11 technology includes the detailed water quality model Ecolab which is needed for the simulation of nutrient contribution to the flood cells of the Delta. At least the first of these Mike

11 models have been coupled to 2D and 3D model on the Coast and in the main River channel. The SIWRP's Mike11 model network of the Mekong delta is presented in Figure 12 (DHI, 2015, Volume 1).

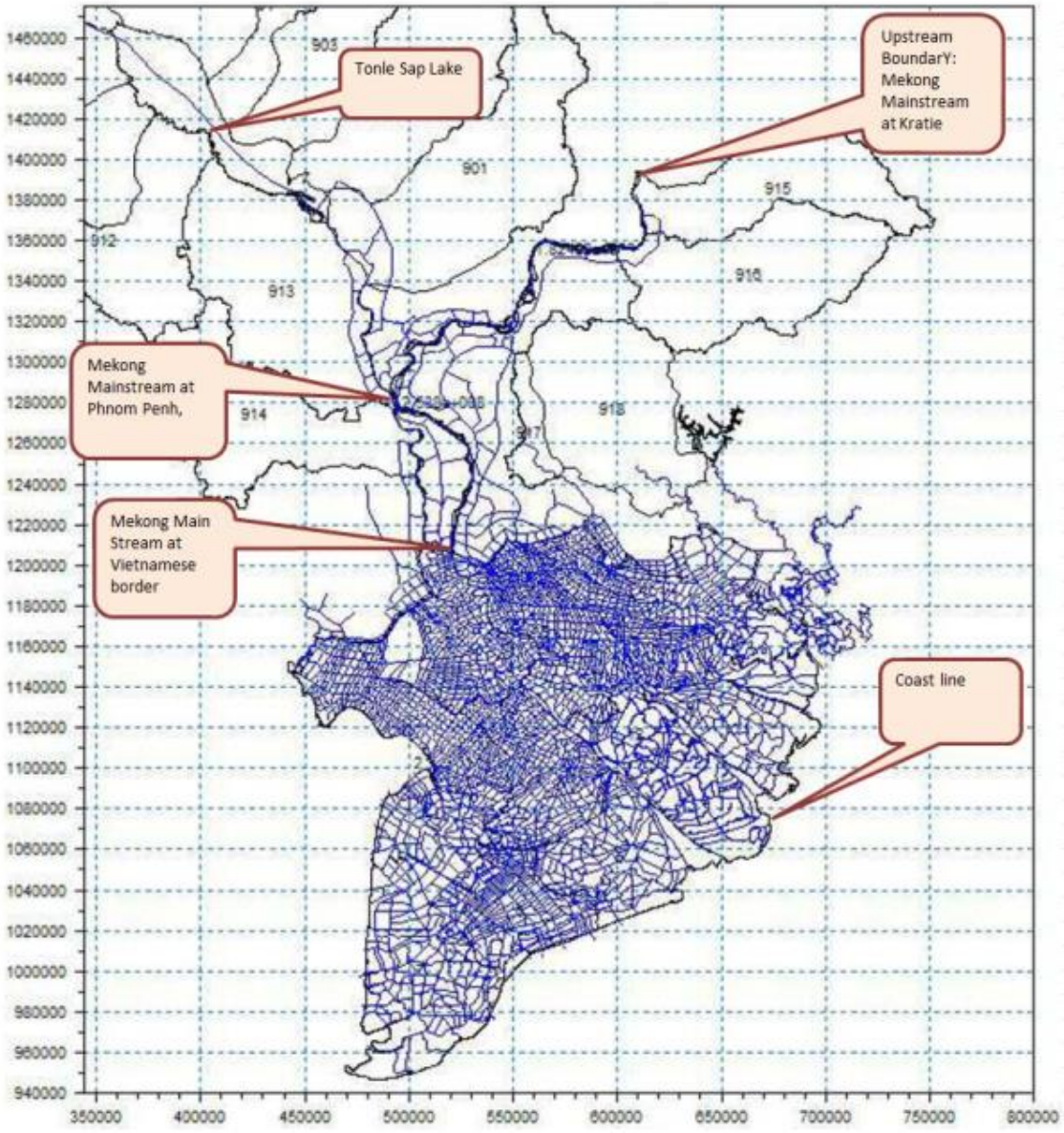

Figure 12: Layout of SIWRP's Mike11 model of the Mekong delta.

Integration of modelling components

Integration with biodiversity models

Species distribution models (SDMs) seek to correlate, using different mathematical forms, the occurrence or geographical location of species with the environmental characteristics of those locations. Through this correlation, large scale predictions of species' habitat suitability can be made. Commonly environmental parameters used in SDMs are climatic, topographic and land cover variables. Applying SDMs for freshwater biodiversity at large scales implies some challenges since environmental

parameters related to the stream network are usually available for particular locations only, are difficult to calculate or extrapolate at larger geographical scales, or do not exist. In the SOS-Water project, however, the output of the hydrological models, which are available at high resolution and at large scales, can be integrated for the first time, as environmental predictors for the SDMs, to understand their influence on the habitat suitability of the fish species in all case studies (Figure 13). Also, projections of those hydrological parameters, given a set of potential scenarios, can be used to estimate changes of species habitats and therefore facilitate the establishment of freshwater biodiversity conservation priorities.

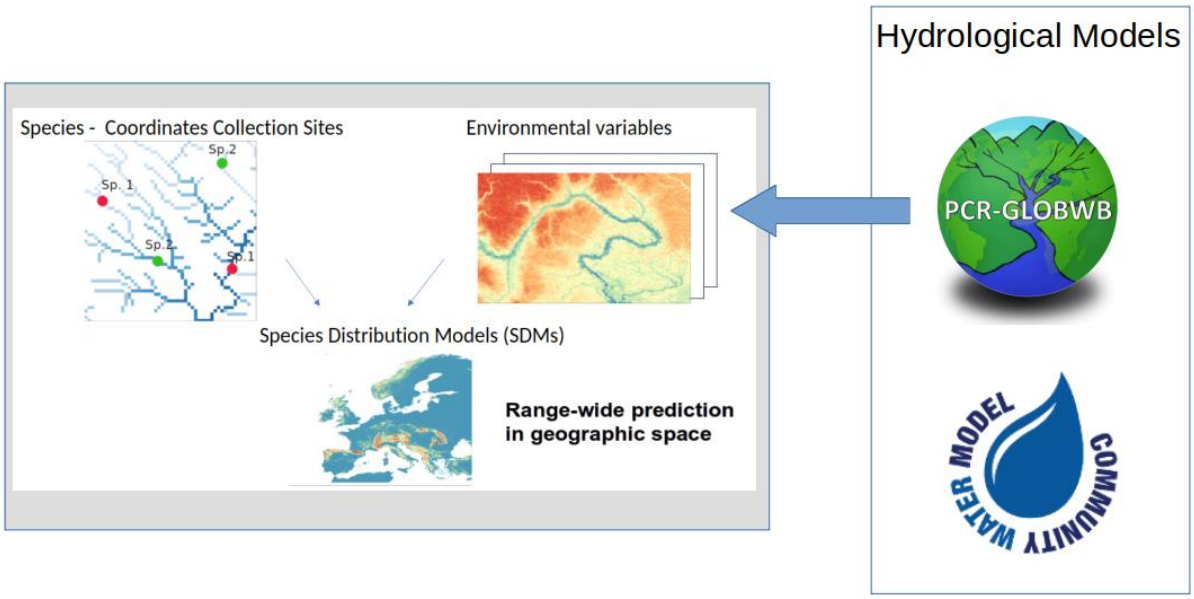

Figure 13: Integration of the output of the hydrological models as environmental variables for species distribution models as an approach to improve the habitat suitability predictions of freshwater biodiversity

The initial habitat suitability maps presented in the results were obtained by including the mean and the standard deviation of water discharge (i.e., yearly average for 2019) for each of the subcatchments in all the case studies. The next steps in the biological modelling workflow involve the inclusion of temporal series for discharge and different yearly statistics (e.g., quantiles).

Integration with Sediment Transfer

In the upper part of the Mekong River Basin, the integration of hydrological components with sediment transport dynamics is achieved through the hard-coupling of VIC-Res and D-CASCADE, creating a comprehensive framework that unifies hydrological processes, water and sediment reservoir management, and sediment connectivity. Beyond simply linking the two models, modifications were necessary to enhance the description of these systems. Notably, to better represent sediment management operations in VIC-Res (in addition to the existing water release management), the reservoir management module was enhanced to include two sediment release strategies: drawdown flushing and sluicing.

Each reservoir within this framework is now characterized by a two-phase state: liquid and solid. At each time step, the integrated framework computes the two-phase mass balance of each reservoir, accounting for both water and sediment volumes entering the impoundment. It then determines the

quantities of water and sediment exiting the reservoirs based on the applied management policies. The full supply storage capacity of a reservoir specifically refers to the water volume it can hold. Consequently, at each time step, the original storage capacity is adjusted to account for the sediment deposited in the reservoir, meaning that only the remaining portion of the initial volume can be filled with water.

The hard-coupling of VIC-Res and D-CASCADE enables continuous communication between the models at every daily time step, facilitating the exchange of feedbacks. VIC-Res provides the daily flow data needed by D-CASCADE to simulate sediment transport and changes in river morphology, while D-CASCADE supplies VIC-Res with daily data on sediment deposition in each reservoir. This feedback influences the two-phase mass balances of the reservoirs, their releases, and ultimately the river flows at the next time step (Figure 14).

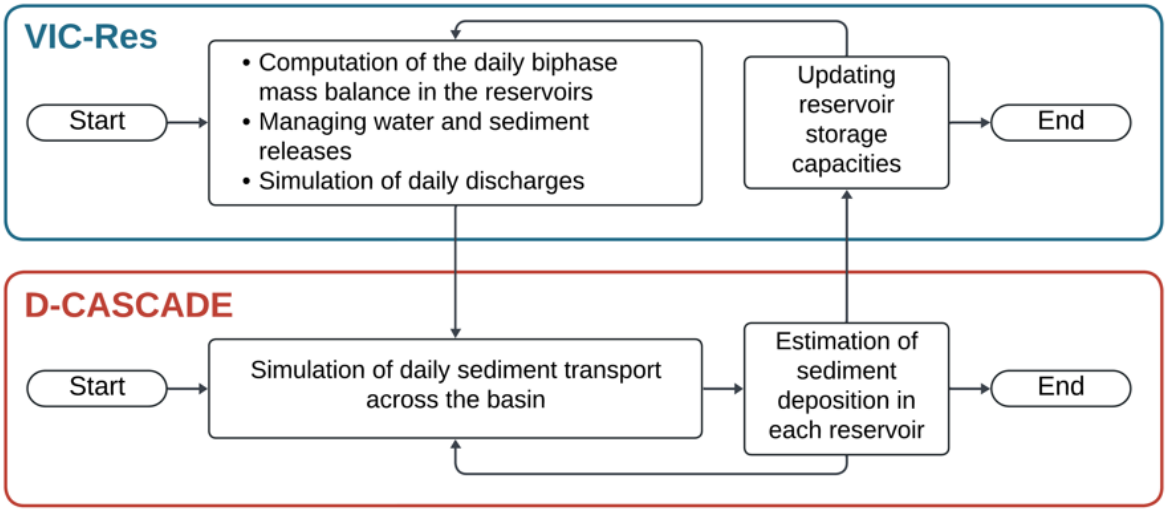

Figure 14: Schematic that shows the hard coupling between Vic-Res and the sediment transport model: D-CASCADE

In addition to linking VIC-Res to D-CASCADE, we are also in the process of linking this combined model to the two localized models in the Mekong Delta: VRSAP and Mike11-St (Figure 15). The main linkage point is at either Kratie (VRSAP) or Pakse (Mike11) two upstream river locations. As VIC-Res is primarily focused on water flows, the resulting values can be easily input as boundary conditions to the VRSAP model. The results of the D-CASCADE sediment transport are readily integrated into Mike11-St to observe the impact of the sedimentation on the delta with a specific focus on land subsidence. This additional linkage allows us to have a stronger understanding of the upstream impacts on water availability in the Mekong Delta and the resulting socioeconomic impacts.

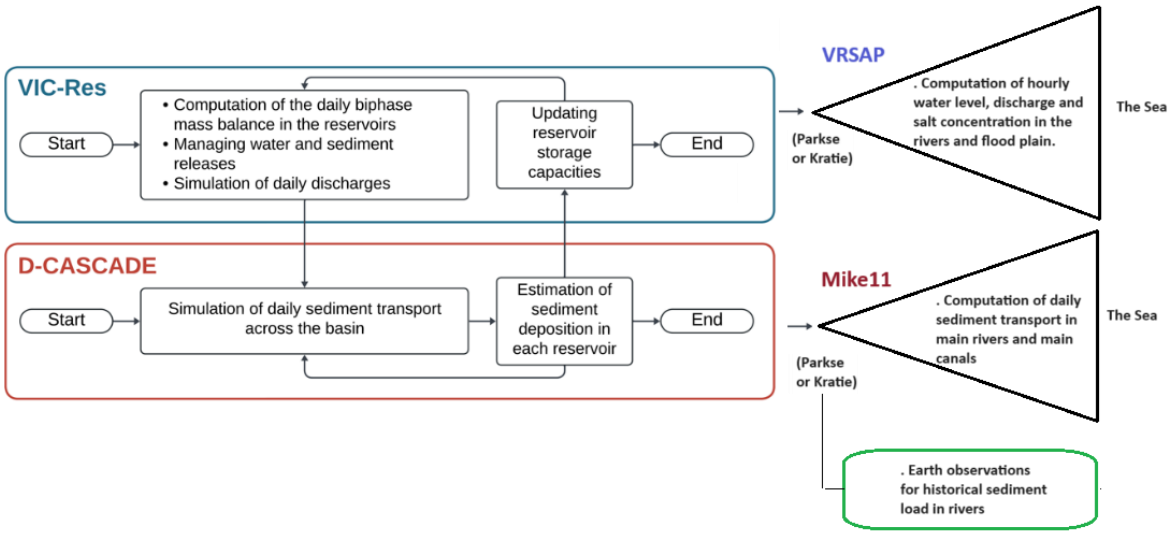

Figure 15: Linkage of Mekong delta models and upstream Mekong models

Validation Datasets/Observational Data

Danube

The three components of the hydrological cycle validated in CWatM are: river discharge, reservoir storage and evapotranspiration. These three components have been benchmarked against publicly available datasets. Ongoing work is preparing datasets on Snow-Water Equivalent (SWE) derived from remote sensing. This dataset will be used to refine the glacier and snow melting routines in CWatM.

Discharge

The datasets used to calibrate the discharge simulated with CWatM in the Danube basin are listed in Table 1. The datasets encompass discharge data from over 1230 gauging stations. The distribution of the stations is shown in Figure 17, in the Validation Dataset section.

Table 1: lists the datasets used for calibrating the discharge in CWatM.

Data source	Web link	Stations
The Global Runoff Data Centre, 56068 Koblenz, Germany	https://grdc.bafg.de	323
Bundesministerium für Land- und Forstwirtschaft, Regionen und Wasserwirtschaft Wasserhaushalt (HZB)	https://ehyd.gv.at/	>500
Bundesamt fuer Umwelt BAFU	https://www.hydrodaten.admin.ch	5
Bavarian State Office for the Environment (LfU)	https://www.lfu.bayern.de/umweltdaten/geodatendienste/index.htm	>100
State Agency for the Environment Baden-Württemberg	https://udo.lubw.baden-wuerttemberg.de	>100
International Commission for the Protection of the Danube Basin	https://www.danubehis.org/	>200

Reservoir storage

Reservoirs and lakes are integrated in CWatM as components of the channel network (Burek et al., 2020). Three distinct historical datasets were used for a comparative analysis against our model results:

1. Hydroweb
2. Sentinel-3A/B
3. GloLakes

Hydroweb offers long-duration time-series of the levels of large lakes with surface areas over 100 km2, reservoirs and 11.336 measurements points on rivers on all continents (Li et al., 2020; https://www.theia-land.fr/en/hydroweb/). The dataset used to calibrate CWatM consists of altimetry data for around 400 channels along the Danube, spanning from 2016 to 2023.

Sentinel-3 is an Earth observation satellite series developed by the European Space Agency as part of the Copernicus Program (https://sentinel.esa.int/web/sentinel/copernicus/sentinel-3). The Sentinel-3A and 3B (S3A/B) satellites are equipped with precise instruments designed to measure surface topography, sea and land surface temperatures, and ocean and land surface color (Kittel et al., 2021). We compared the data to the channel storage and reservoir storage values generated by CWatM using 360 measurement points from S3A/B.

The GloLakes dataset provides historical and near-real-time time series of relative (i.e. storage change) and absolute (i.e. total stored volume) storage for more than 27, 000 lakes worldwide using multiple sources of satellite data, including laser and radar altimetry and optical remote sensing (Hou et al., 2024).

Evapotranspiration

Evapotranspiration (ETa) is a fundamental component of the water cycle. In CWatM, ETa is calculatedby first computing the Potential Evapotranspiration (ETp) and then by multiplying ETp by a land-cover dependent crop coefficient (Kc). ETa simulated in CWatM was benchmarked against the remote sensing products in Table 2. Benchmarking was conducted for the period 2014-2020, utilizing raster images obtained from publicly accessible repositories. A stratified sampling approach was employed, with varying numbers of images downloaded across different months to account for seasonal variations in evapotranspiration. Specifically, two images were acquired for winter months (January, February, November, and December), three for spring and autumn (March, September, and October), and three to five images for summer months (June, July, and August), depending on data availability. This stratification reflects the higher importance of evapotranspiration during the spring and summer months. To have a consistent comparison between CWatM-simulated ETa and remote sensing products, the CWatM ETa data were aggregated into 8-day averages and 8-day sums to match the temporal resolution of the MODIS 1km and Penman-Monteith-Leuning datasets, respectively (see Table xxx). In contrast, no aggregation was necessary for direct comparison with ET Monitor. Data extraction from CWatM ETa and remote sensing products was conducted using a 30 km regularly spaced grid of points with a total of 381 points. For each grid point and time step where data was available, the simulated ETa values from CWatM and the corresponding ETa values from the remote sensing products were extracted. KGE metric was calculated for each remote sensing product at each grid point, utilizing the corresponding CWatM-simulated ETa values as per Table 2.

Table 2: ETa datasets used to benchmark ETa simulated with CWatM and corresponding CWatM aggregated dataset.

Product	Time step	CWatM ETa	Data source	Reference
ET Monitor (352 images)	daily	ETa-daily	https://data.casearth.cn/thematic/GWRD_2023/272	Zheng et al. 2022
Modis 1km (45 images)	8 days sum	ETa-8days sum	https://developers.google.com/earth-engine/datasets/catalog/MODIS_NTSG_MOD16A2_105	Qiaozhen et al. 2014
Penman-Monteith-Leuning (321 images)	8 days mean	ETa-8days mean	https://developers.google.com/earth-engine/datasets/catalog/CAS_IGSNRR_PML_V2_v018#description	Zhang et al., 2019, Gan et al., 2018, Zhang et al., 2016

Uncertainty

The main device implemented to address uncertainty in the modelling of the Danube basin was the use of 5 different hydrometeorological inputs datasets (e.g. precipitation, temperature, wind speed etc.) from five different Global Circulation Models (GCMs). Using a GCMs ensemble systematically

addresses the inherent biases and uncertainties of individual climate projections. By drawing on diverse mathematical representations and parameterizations, ensemble predictions capture a wider range of climatic variability than a single model might. This approach allows for the quantification of CWatM uncertainty, making projections more robust and less susceptible to individual GCM errors. Key benefits include improved reliability, comprehensive uncertainty representation, and a broader range of potential outcomes.

The five GCMs used as meteorological forcing for CWatM and following the ISIMIP3b (Inter-Sectoral Impact Model Intercomparison Project) protocol are from the CMIP6 (Coupled Model Intercomparison Project Phase 6) generation and encompass:

- GFDL-ESM4
- IPSL-CM6A-LR
- MPI-ESM1-2-HR
- MRI-ESM2-0
- UKESM1-0-LL

Jucar

The validation period chosen comprises 14 full years, from October 1998 to September 2012. This period provides a consistent picture in terms of infrastructure development, governance and water planning and management, overlapping with the reference period of CMIP6 scenarios (1979-2014). The following monthly-scale datasets and information sources have been used:

- Reservoir datasets: historical records on storage and releases have been obtained from the database of the Centre for Hydrological Studies of Spain (*Anuario de Aforos del CEDEX*, https://ceh.cedex.es/anuarioaforos/default.asp) and directly provided by the Jucar River Basin Agency. Both sources coincide. Although the datasets collected refer to all the reservoirs placed in the Jucar river basin, only Alarcon, Contreras and Tous were considered relevant for model validation.
- Streamflow datasets: historical records on streamflows in gauging stations have been obtained from the database of the Centre for Hydrological Studies of Spain. In particular, the model validation has been conducted in seven gauging stations with automatic measurement systems placed in the Jucar and Cabriel rivers, plus one derivative observation of the stream-aquifer interaction obtained measured the difference between two gauging stations, in order to evaluate how the model reproduces the stream-aquifer interaction between the Jucar river and the Mancha Oriental aquifer.
- Delivery datasets: historical records on deliveries to eight consumptive demands, plus the discharge of the Jucar to the Mediterranean Sea, have been obtained from the Automatic System for Hydrological Information (*Sistema Automático de Información Hidrológica*, SAIH) of the Jucar River Basin Agency. These deliveries refer to the main surface water allocations placed downstream of the Alarcon and Contreras reservoirs, with the exception of the supply to the Cofrentes nuclear power plant (which is granted).
- Albufera datasets: the main reference water balance components of the Albufera wetland, at the annual scale, were obtained from CHJ (2023). These were, in turn, derived using a detailed

mathematical model of the water stocks and fluxes found in the wetland, whose complexity required significant simplifications in order to fit into a basin-scale water resources management model.

Mekong

Upper Basin - Upper and Lower Mekong excluding the Delta

The VIC-Res hydrological model requires a broad range of input data, summarized in Table 3. Precipitation and temperature datasets have a spatial resolution of 0.25°, while our VIC-Res implementation operates at a resolution of 0.0625°. To address this difference, we employed the bilinear interpolation method to upscale the data (Dang et al., 2020). Land use and soil datasets have a resolution of 30 arc seconds and were processed using the majority resampling technique, which assigns the most common value among a group of pixels to a new cell.

Table 3: VICRes Input Data Sources

Input data	Data Source
Daily Rainfall	Climate Hazards Group InfraRed Precipitation (CHIRPS)
Daily Temperature (maximum and minimum)	Climate Hazards Group InfraRed Precipitation (CHIRTS)
Land use and land cover data	Global Land Cover Characterization dataset
Soil data	Harmonized World Soil Database
Monthly Leaf Area Index	Terra MODIS satellite images
Albedo	Terra MODIS satellite images
Flow direction map	GTOPO30 Digital Elevation Model

For this deliverable, we conducted an initial calibration using only the observed daily discharge at Stung Treng (obtained from the Mekong River Commission data portal) for the period 1996 to 2005, while the years 2006 to 2010 were used for validation. With this dataset, we calibrated six parameters of the rainfall-runoff model across the entire domain covered by the model.

Further improvements in model performance will rely on a refined calibration scheme based on additional gauging stations with available daily discharge data. The basin will be divided into eight sub-basins (Chiang Saen, Ubon, Ban Kengdone, Ban Tha Kok, Vientiane, Mukdahan, Pakse, and Stung Treng), and the six rainfall–runoff parameters will be calibrated for each of them, resulting in a semi-distributed parameterization instead of a single-basin approach.

Concerning D-CASCADE, a key input is the baseline sediment budget, which represents the amount of sediment available in the basin for mobilization. Due to the lack of specific distributed field data, we defined this baseline by running D-CASCADE under various sediment budget scenarios, varying both the total annual sediment supply to the basin and their grain-size distributions. We then selected

scenarios that successfully reproduced the historical average annual sediment loads observed at five river sections, which served as our calibration and validation dataset.

These sediment loads were obtained by processing data from the Mekong River Commission's portal and the DSMP 2009-2013 (Koehnken, 2014). Additionally, we leveraged the work of De Xun Chua and Xi, 2022 , who used these data to estimate annual sediment loads for six stations on the Mekong River from 1965 to 2019, enabling us to reconstruct our calibration and validation datasets. Specifically, we selected five stations well-distributed along the river network: Chiang Saen, Luang Prabang, Nong Khai, Khong Chiam, and Kratiè. We differentiated three periods: pre-dam (1965-1991), growth (1992-2008), and mega-dam (2009-2019), thus reconstructing the calibration dataset (pre-dam and growth) and the validation dataset (mega-dam). The mega-dam period saw the operation of many new dams along the river, allowing us to also test the model's accuracy in representing the reservoirs' trap efficiency.

The model was calibrated to reproduce the sediment load at Kratiè, even though the closure section is located few kilometers upstream. This ensures that the outputs of our model can be used as boundary conditions for the models operating in the delta managed by SWIRP partners.

The core model structures for both the rainfall–runoff and D-CASCADE components were already available prior to this project. Within the project, only minor structural adjustments were introduced to ensure their suitability to the Mekong Basin and to the project's objectives. The main effort focused on calibration and validation activities—some of which are still ongoing, as detailed below—to ensure the models can be reliably applied to the specific settings of the project.

At this stage, the main modelling structures and preliminary calibrations have been completed within the project. The next steps before full application to risk assessment within the **Safe Operating Space framework** include:

- Completing sub-basin-based calibration and validation of the rainfall–runoff model using additional gauging stations;
- Refining sediment budget estimates with new field or satellite data, where available;
- Integrating the calibrated models into the broader system analysis for risk assessment and scenario evaluation.

Mekong Delta

VRSAP model

Hydrological data for model validation include hourly water levels at 30 stations in the Mekong Delta, including 5 flow measurement stations on the Mekong mainstream (Tan Chau, Chau Doc, My Thuan, Can Tho, and Vam Nao stations). The model is validated with typical years for the rainy season (flooding and drainage) and the dry season (drought and salinity intrusion). The flood season is selected as the most recent historical flood in 2011 and the most recent relatively large floods in 2018 and 2020. The dry season is validated with data from extreme years such as 2008, 2016, 2020 and some additional measurement stations in April 2023.

Mike11-ST model

Suspended sediment data in the Mekong Delta are available at five regular hydrological measuring stations on the mainstream (Tan Chau, Chau Doc, Vam Nao, My Thuan, Can Tho). SIWRP is surveying suspended sediment and bedload at many canal locations (SIWRP, 2021, Hydrology and water

resources report for the Mekong delta). In 2024, surveying is in a part of the western coastal area (Ca Mau Peninsula). All relevant station information is shown in Figure 16.

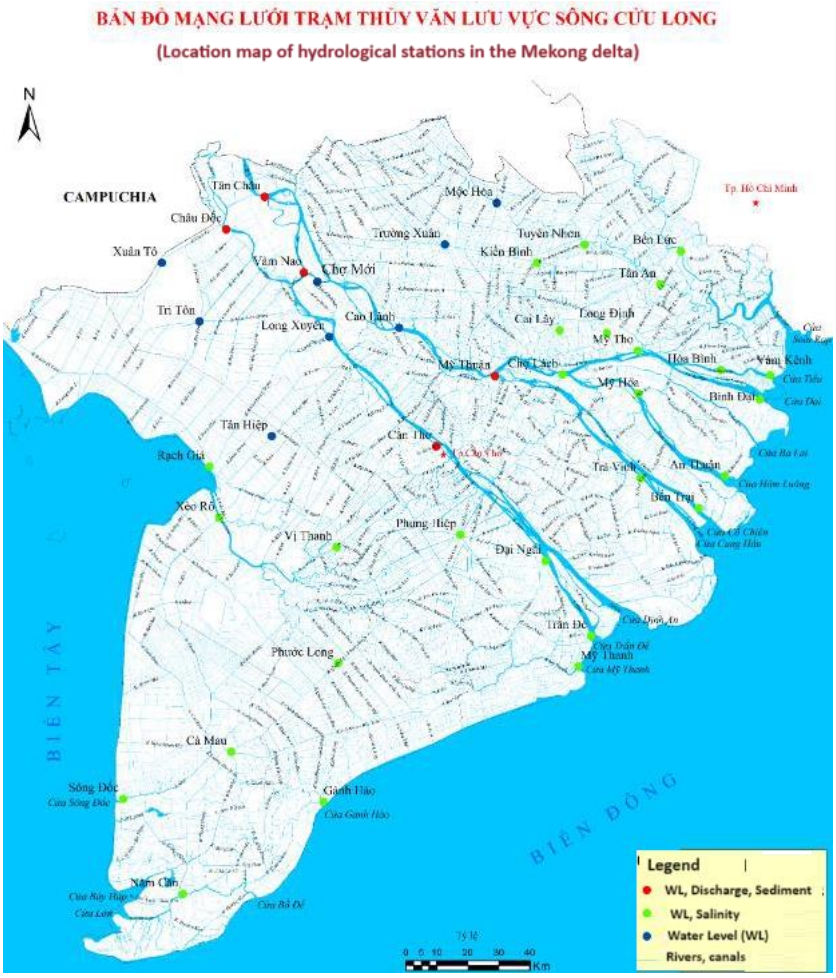

Figure 16: Location map of hydrological stations in the Mekong delta for model calibration

Rhine

To independently validate the changes in PCR-GLOBWB 2.0, we use two main types of datasets: direct observations of streamflow and remotely sensed data of reservoir storage and total water storage. The first is global discharge data from the Global Runoff Data Centre (GRDC, 2020, https://www.bafg.de/GRDC) (last access: 1 Aug, 2024), total liquid water equivalent data from GRACE-FO (Landerer et al., 2020) and reservoir storage data from GloLakes (Hou et al., 2024). The Global Runoff Data Centre contains over 10,000 gages globally and is a key validation dataset for global hydrological models because of this. Along the Rhine, GRDC has 19 gages that cover all three subbasins: the upper basin (13 gages), the middle basin (5 gages) and lower basin (1 gage). Therefore, we can validate the discharge from our integrated water modeling framework across the entire Rhine River. We used the liquid water equivalent in GRACE-FO to evaluate the total water stored in both groundwater and surface water for PCR-GLOBWB 2. While these values are not exactly identical, as GRACE-FO primarily looks at gravity changes and links those to water storage, they can be used to directly evaluate long term trends. GloLakes contains remotely sensed reservoir storage data for over

22,000 reservoirs and lakes throughout the globe and therefore is a key dataset to evaluate our storage changes against. In the Rhine, GloLakes contains 1754 reservoirs within the full Rhine basin.

The underlying PCR-GLOBWB2 model at the 1km resolution was already readily available from two paper publications: Hoch et al., 2023 and van Jaarsveld et al., 2024. Initial calibrations with GRDC streamgages at Lobith NL, Andernach, DE and Basel, CH were performed to determine which of the two modelling frameworks were most suitable for our analysis of the Rhine. This was because the modelled evapotranspiration in the most recent version of the 1km PCR-GLOBWB2 model resulted in higher evaporative losses from vegetation and therefore decreased the streamflow accuracy. We also validated the updated reservoir scheme against observations from GLoLakes to ensure our modelled reservoir storage captured an accurate average storage and the seasonalities. As with the Danube as well as the other case studies, the main avenue to address uncertainty in the Rhine modelling framework was through the implementation of the GCM model ensembles.

Results

Danube

Discharge, storage and evapotranspiration benchmarking of CWatM simulations were evaluated using the Kling Gupta Efficiency (KGE) index. KGE is a dimensionless index used to evaluate the performance of hydrological models. It considers three aspects of model performance: correlation, bias, and variability. A KGE value of 1 indicates perfect model performance, while a value of 0 suggests no correlation between simulated and observed values. KGE values above 0.6 are considered satisfactory and above 0.8 excellent.

Discharge

The evaluation of CWatM demonstrated satisfactory performance across the Danube Basin (Figure 17), with 444 out of 581 stations (76%) achieving a KGE score of 0.6 or higher. Notably, 228 stations (39%) exhibited excellent performance with KGE values exceeding 0.8. While 137 stations (24%) displayed KGE scores below 0.6, and 33 stations yielded negative KGE values, these results are largely attributable to specific regional challenges. In the alpine region, the inclusion of glacier dynamics using the OGGM model significantly enhanced model accuracy, as exemplified by Innsbruck INN with a KGE of 0.94. Conversely, the Morava and Tisa regions exhibited suboptimal performance due to factors such as water transfers, unaccounted channel systems, and unaccounted agricultural water withdrawals. Overall, the model demonstrated robust capabilities in capturing the complex hydrological processes within the Danube Basin.

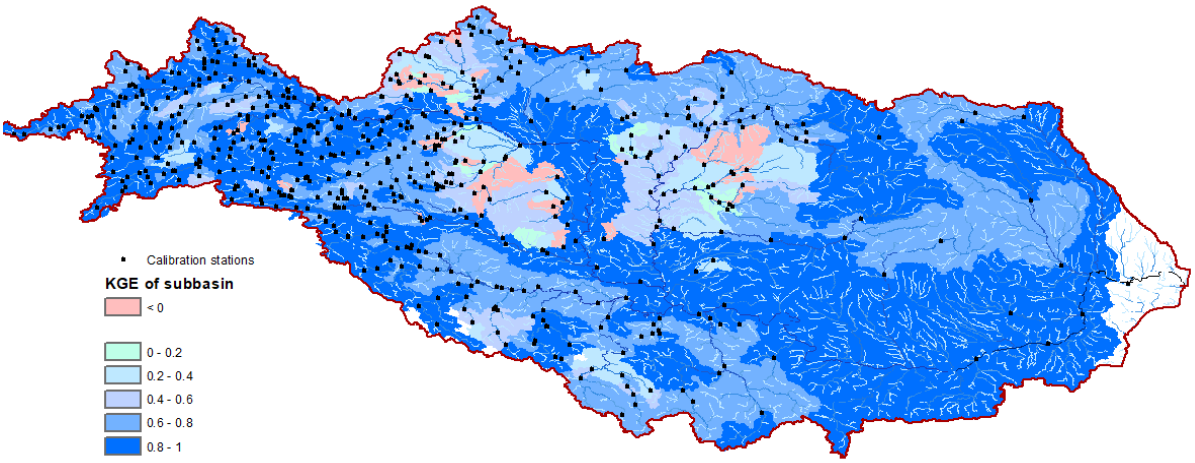

Figure 17: Calibration results (KGE) for the Danube of 581 calibration stations

Reservoir storage

The average correlation for the channel volumes simulated with CWatM and the Hydroweb dataset exhibited medium-high values for almost half of the measurement stations (46%). The correlation values for Sentinel-3A/B showed medium-low values for both channel storage and reservoir storage. The correlation between the GloLakes dataset and CWatM simulated reservoir storage output performs better than for the other datasets, especially when considering the comparison between CWatM at 1 arc-min resolution and big lakes and large reservoirs (see Figure 18).

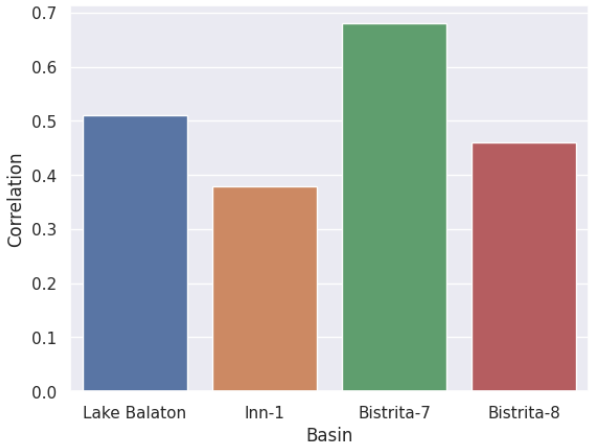

Figure 18: Correlation between GloLakes and examples of reservoir storage simulated with CWatM

The results of the reservoir storage comparison must consider the limitations arising when comparing satellite-derived reservoir storage from GloLakes with CWatM simulations:

First, GloLakes relies on simplified empirical area-volume relationships to estimate storage, which can introduce substantial errors in volume estimation, particularly for reservoirs with complex bathymetry or non-standard geometries.

Second, the temporal resolution of satellite observations presents challenges. The available time series contained relatively long gaps, limiting the ability to capture short-term filling and emptying dynamics.

This is particularly relevant during the spring season in the Danube Basin, when rapid snowmelt-driven inflows and subsequent releases occur.

Third, the CWatM version used in that analysis employed a simplified rectangular reservoir geometry, assuming constant surface area regardless of storage level. Subsequent model developments have incorporated Volume-Elevation-Area relationships derived from satellite bathymetry, providing a more physically consistent representation of reservoir storage. A reassessment using the updated model configuration remains to be conducted.

Evapotranspiration

Figure 19 presents the results of the ETa benchmarking analysis. The upper panel in Figure 19 depicts cumulative distribution curves for the KGE metric relative to each remote sensing product. The lower panel in Figure 19 illustrates the correlation between simulated and observed ETa values. For most sampled points, both KGE and correlation coefficients exhibit high or very high values, indicating the CWatM model's proficiency in accurately simulating the ETa component of the Danube Basin's water cycle.

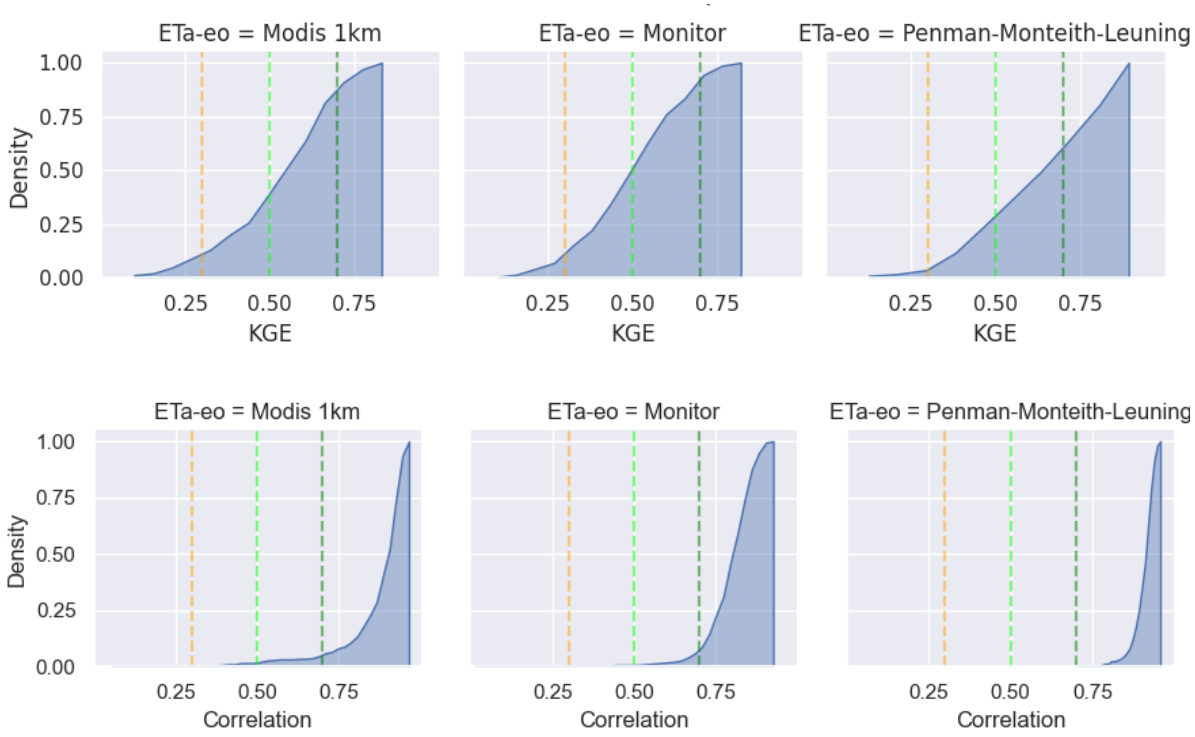

Figure 19: KGE cumulative distribution of the ETa simulated with CWatM vs. remote sensing products.

Danube results summary

The structural evolution of the CWatM hydrological model increased physical complexity and spatial scalability. CWatM now integrates the Open Global Glacial Model (OGGM) and refines reservoir operation algorithms. These changes help capture cryospheric and anthropogenic influences on water cycles more accurately. Further, optimized source code routines allow the model to process 1' spatial resolution data. This enhancement supports managing a substantial increase in grid cells caused by higher spatial resolution while maintaining acceptable computational efficiency. See

section Methodology/Methodology-Danube for a detailed description of the datasets and references.

Calibration and validation of CWatM for the Danube case study used a multi-source data assimilation approach (Table 4). High-fidelity crop maps and irrigation calendars help refine the simulation of human water demand. Discharge calibration used an extensive dataset of 581 stations, including data from the DanubeHIS and regional Bavarian and Baden-Württemberg services. Volume validation for channels and reservoirs combines Hydroweb, Sentinel-3A/B altimetry, and the GloLakes dataset. The model's energy balance is validated by benchmarking actual evapotranspiration against ET Monitor, MODIS, and Penman-Monteith-Leuning products to ensure an accurate water balance. See the Validation Datasets/Observational Data-Danube section for details on the datasets and references.

Table 4: datasets used to validate the enhanced CWatM version across different hydrological variables

Variable	Dataset / Source	Purpose
Water Demand	Detailed Crop Maps & Irrigation Calendars	Accurate irrigation requirements and scheduling.
Discharge	581 Stations (DanubeHIS, LfU, LUBW)	Calibration of river flow and runoff.
Channel/Reservoir Volume	Hydroweb, Sentinel-3A/B, GloLakes	Validation of storage dynamics and water levels.
Evapotranspiration (ET_a)	ET Monitor, MODIS 1km, Penman-Monteith-Leuning	Validation of surface flux and water loss.

Although further enhancements such as the implementation of water transfer rules or the increase of the discharge stations dataset are ongoing and, more generally, constant developments and improvements are part of the normal life cycle of a model, given the satisfactory calibration and validation performances of the current CWatM settings, no further calibration or validation action is scheduled before applying CWatM in the risk assessment of the SOS.

Jucar

Kling-Gupta Efficiency (KGE) index was the main metric used to evaluate the performance level of the Jucar hydro-economic model for reservoirs, stream flows and deliveries. Given that the Albufera water balance was available at the annual scale, its validation was performed based on visual comparison between the reference datasets and the ones provided by the hydro-economic model.

Reservoirs

The KGE indices achieved by the Jucar hydro-economic model in the main Jucar reservoirs, as well as their combined storage, are shown in the Table 5, while the time series of modelled versus observations for them appear in the following Figure. The values of the indices and components show

an adequate adjustment of the storage levels obtained from the model to the observed ones, in particular for the combined storage of Alarcon, Contreras and Tous. This last reservoir shows the lowest KGE coefficients due to a weaker correlation and standard deviation terms, although the achieved performance is satisfactory.

Table 5: KGE indices and components for the adjustment of main reservoir storages of the Jucar hydro-economic model

Reservoir	r	μ	σ	KGE
Alarcon	0.94	0.99	0.85	0.84
Contreras	0.94	0.89	1.04	0.86
Tous	0.77	1.06	0.71	0.62
A+C+T	0.95	0.97	0.89	0.87

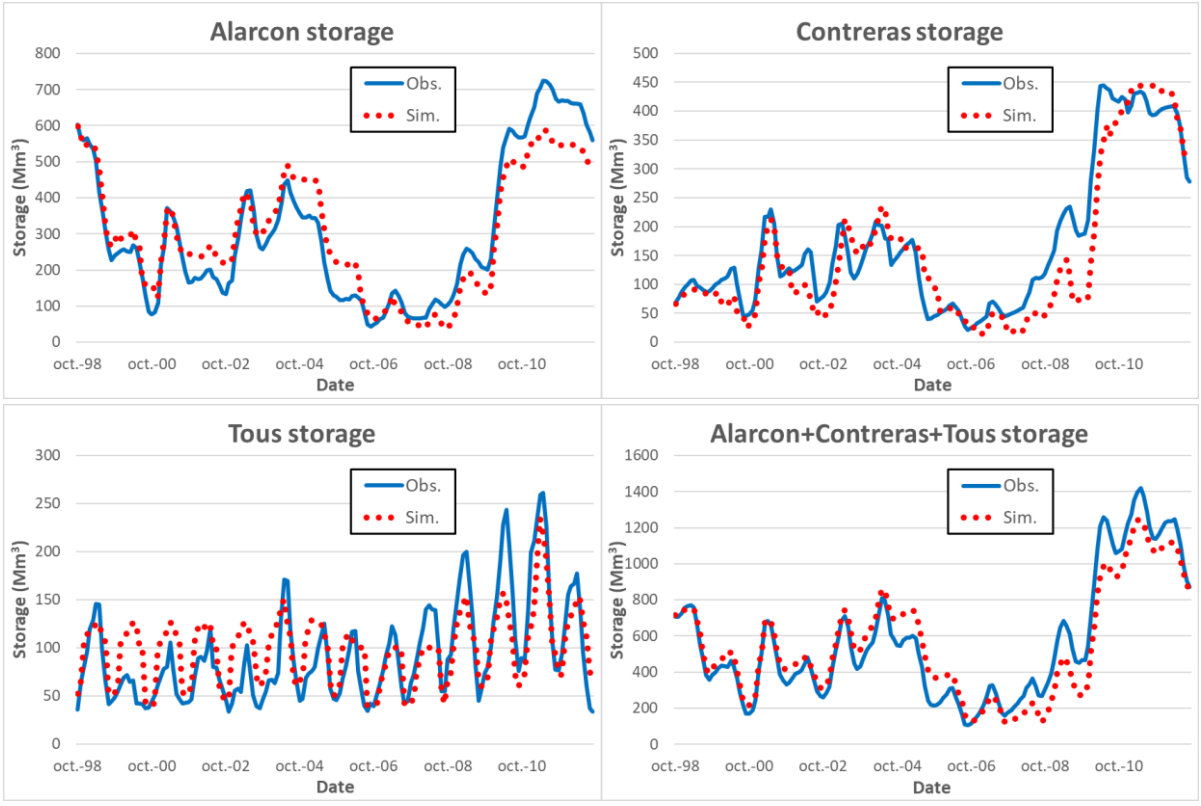

Figure 20: Reservoir storages comparison plots between the Jucar hydro-economic model and observations

The corresponding KGE indices and associated terms for the representation of reservoir releases, as well as the time series plots, are presented in the Table 6 and Figure 20. Performance levels show a decrease compared to storages, which was expected since the temporal dependency of releases is lower than the one on storages. In any case, with the exception of Contreras, the metrics achieved are considered adequate. The model finds it challenging to reproduce the monthly releases from Contreras, although the fact that Contreras storages are fairly reproduced suggest that the model behavior at seasonal and annual time scales is better. The combined releases from Alarcon and Contreras, which directly influence the water balance of the middle and lower Jucar, is adequately

reproduced (Figure 21). Similarly, the releases from Tous show the best performance level, which is particularly relevant since it is the reservoir placed immediately upstream the main surface demands.

Table 6: KGE indices and components for the adjustment of main reservoir releases of the Jucar hydro-economic model

Reservoir	r	μ	σ	KGE
Alarcon	0.70	0.88	1.07	0.67
Contreras	0.42	0.69	0.75	0.30
Tous	0.89	0.91	0.77	0.73
A+C	0.71	0.80	0.86	0.63

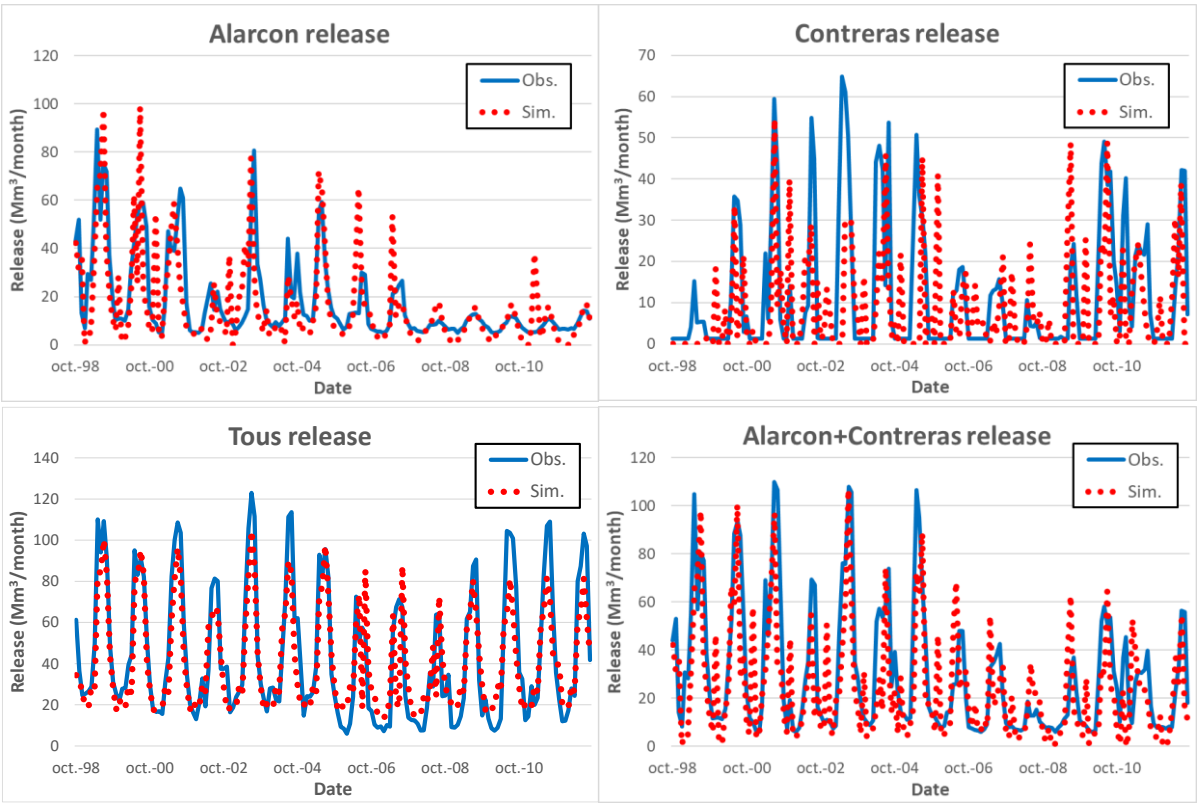

Figure 21: Reservoir releases comparison plots between the Jucar hydro-economic model and observations

Streamflows

The KGE and associated terms and the time series plots can be found in Table 7 and Figure 22. With the exception of the reproduction of the stream-aquifer interaction between the Jucar river and the Mancha Oriental aquifer, which shows a negative KGE, the performance level is adequate. The reason behind the negative KGE in the stream-aquifer interaction is its complexity, which challenges a basin wide model. In any case, the plot shows that the model reproduces the intra-annual cycle of stream-aquifer exchanges, plus providing adequate results in a significant number of the historical years, in particular the last ones. Among the locations with positive KGE values, the Cofrentes and Los Frailes gauges show the lowest values, being the only ones below 0.50. The reason why seems to be the

challenging reproduction of the Contreras releases (upstream of the Cofrentes gauge) and the stream-aquifer interaction for the Los Frailes gauge.

Table 7: Reservoir releases comparison plots between the Jucar hydro-economic model and observations

Location	Sub-basin	River	r	μ	σ	KGE
El Picazo	Middle	Jucar	0.68	1.04	1.02	0.68
Los Frailes	Middle	Jucar	0.57	0.70	0.97	0.47
Alcala del Jucar	Middle	Jucar	0.61	0.89	1.02	0.60
Mancha stream-aquifer	Middle	Jucar	0.71	2.58	0.74	-0.63
Cofrentes	Middle	Cabriel	0.43	0.93	1.14	0.41
Tous	Lower	Jucar	0.88	0.90	0.80	0.74
Antella	Lower	Jucar	0.58	0.92	0.79	0.52
Huerto Mulet	Lower	Jucar	0.79	0.99	0.76	0.69

KGE indices and components for the adjustment of streamflows of the Jucar hydro-economic model

Figure 22: Streamflow comparison plots between the Jucar hydro-economic model and observations

Deliveries

The performance achieved by the hydro-economic model in reproducing the historical observations on surface demands is included in the Figure 23 and Table 8a. The discharges to the Mediterranean Seas, although not a consumptive demand, have been included in this subchapter considering that their information source is the same as the deliveries and differs from the one corresponding to the streamflows shown before. Observations for these variables show gaps caused by change of measuring protocols and addition or removal of items included in the SAIH reports and databases. Except for the discharge to the sea, with a KGE equal to 0.33, the hydro-economic model is fairly reproducing the historical surface deliveries of the Jucar River basin, achieving values higher than 0.80 in some cases. Given that these variables are key in estimating the model's economic performance, an adequate reproduction of them directly impacts the economic results of the Jucar model.

Table 8: KGE indices and components for the adjustment of demand deliveries of the Jucar hydro-economic model

Demand	r	μ	σ	KGE
CJT total	0.78	1.13	0.66	0.58
CJT irrigation	0.88	0.81	0.73	0.65
Escalona	0.86	1.20	0.89	0.73
Acequia Real	0.83	0.90	0.96	0.80
Sueca	0.89	1.01	0.87	0.83
Cuatro Pueblos	0.86	1.09	0.91	0.81
Cullera	0.82	1.01	0.86	0.77
Mancha Oriental surface irrigation	0.70	0.94	0.87	0.67
Sea discharge	0.81	1.63	0.88	0.33

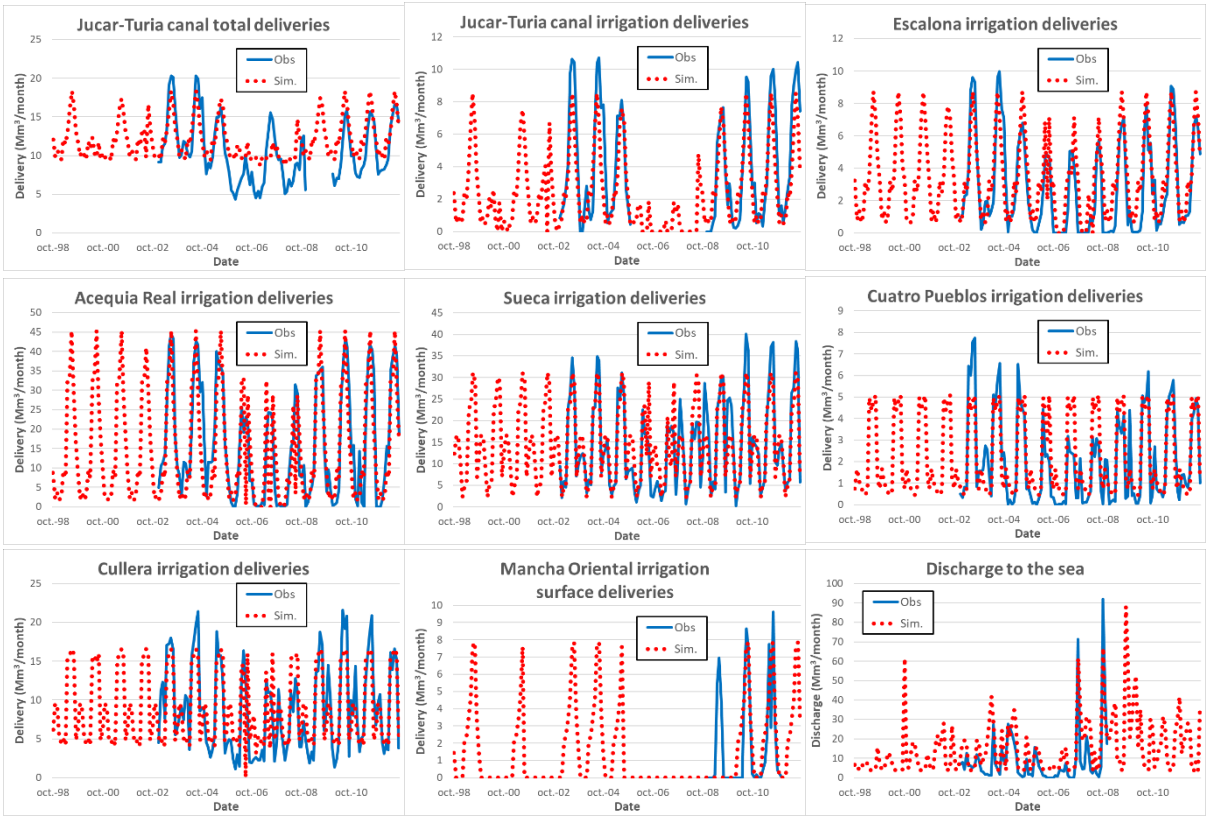

Figure 23: Demand delivery comparison plots between the Jucar hydro-economic model and observations

Albufera water balance

The comparison of annual water balance components provided by the hydro-economic model with those from the Jucar RBA model of the Albufera is presented in the Figure 24, in which both bars and lines show the cumulative inflows to the Albufera. The "Natural" inflows refer to rainfall and hydrological discharge (surface and groundwater) directly related to the Albufera basin, which is a semi-endorheic basin placed between the Jucar and the Turia river basins. To simplify the hydrological modelling, this basin was skipped and the inflows to the Albufera were considered to be equal to a percentage of the hydrological discharge of the neighboring lower Jucar River basin, fixed so that the average annual inflows are the same. As seen in the figure, the inter-annual dynamics are respected in most years, which is considered acceptable taking into account the simplification implemented. The "Jucar" inflows refer to the returns from the agricultural demands of the lower Jucar River basin (both from surface and groundwater) plus the direct water allocation from the Jucar to the Albufera wetland (inexistent in the validation period). The results show a similar behavior as the Natural inflows, being deviations explained by the fact that the model considers returns as a fixed percentage of deliveries, while in reality this ratio is subject to changes across years. The last component, the "Turia" inflows, corresponds to the agricultural returns of the Turia demands located close to the Albufera, which are not modelled by the hydro-economic model of the Jucar. This component is the lowest in quantitative terms, and thus the hydro-economic model considers it equal to 40 Mm3/year, which is the average provided by the Jucar RBA model of the Albufera.

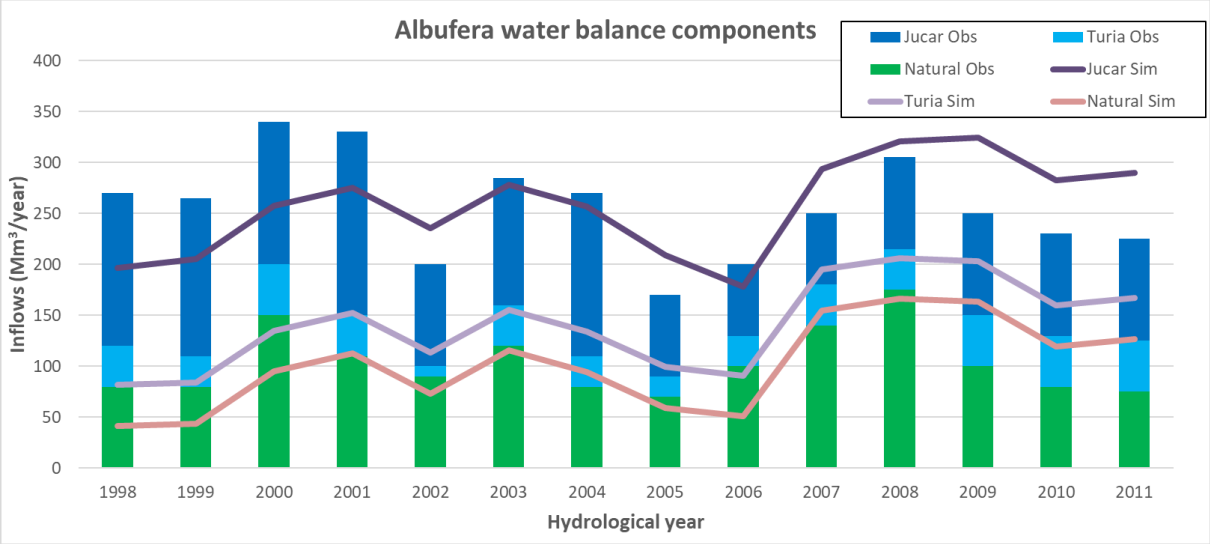

Figure 24: Albufera water balance comparison between the Jucar hydro-economic model and the Jucar RBA model

In summary, the calibration of the Jucar model is deemed adequate for the purposes of SOS-WATER; since deliveries to consumptive demands are well reproduced and, for the rest of the variables that define the SOS, the level of adjustment is good enough to extract trends and impacts of measures in the long-term. Although not being a weakness for the SOS calculation, the model has several points of improvement that could be addressed in the future:

- The water balance of the Albufera wetland has challenges in capturing intra-annual and inter-annual variability of consecutive years, and thus might only be used for analyzing long-term trends and metrics
- The model representation of the middle basin stream-aquifer interaction and streamflow change is improvable, and it should only be used to assess long-term trends as metrics, as happens for the Albufera wetland. In this regard, a further improvement in the embedded multireservoir model of the Mancha Oriental aquifer could be considered.

Uncertainty has been addressed in the same way as the Danube, choosing diverse climate change scenarios and models. In this regard, the Jucar has opted for the same scenarios and models as the Danube, to guarantee that assessments are comparable.

The Jucar model robustness to simulate future climatic conditions not experienced in the past is addressed by adopting a modelling chain that involves hydrological, agronomic and fish habitat models (see deliverable D5.2). These provide input to the hydro-economic model, ensuring a proper representation of key hydrological and agronomic processes and the acknowledgement of future conditions that might not have been found yet in the observations. In particular, hydrological scenarios are obtained using the eco-hydrological model TETIS. This model has been widely used in the assessment of droughts and floods, which guarantees its ability to deal with both hydrological extremes. Similarly, the well established FAO Aquacrop model has been used to assess crop irrigation needs under future climatic patterns. This model has been widely applied across the globe for similar purposes. In fact, future irrigation needs for the Jucar are systematically above the historical ones, in response to growing temperatures.

Mekong

Upper Basin

The current performance of the VIC-Res model, based on the initial calibration using only discharge data from Stung Treng, is illustrated in Figures 25 and 26. The model shows a reasonable ability to reproduce the observed hydrograph at Stung Treng and other stations along the Mekong mainstream (Chiang Saen, Vientiane, Mukdahan, and Pakse). The Nash–Sutcliffe Efficiency (NSE) values range from 0.48 during calibration to 0.58 during validation at Stung Treng, with slightly lower values at the other stations. Although these results cannot be considered fully satisfactory, they are acceptable for a preliminary calibration stage.

As discussed in the calibration sections, further steps are currently being implemented to improve model performance. The ongoing comprehensive calibration—based on multiple gauging stations and sub-basin parameterization—is expected to enhance the model's ability to reproduce both peak and low-flow conditions. While some discrepancies remain in simulating high-flow events, the model already provides a consistent representation of low-flow periods, which are strongly influenced by reservoir management. These results confirm that the model framework is suitable for refinement and further application within the project's context.

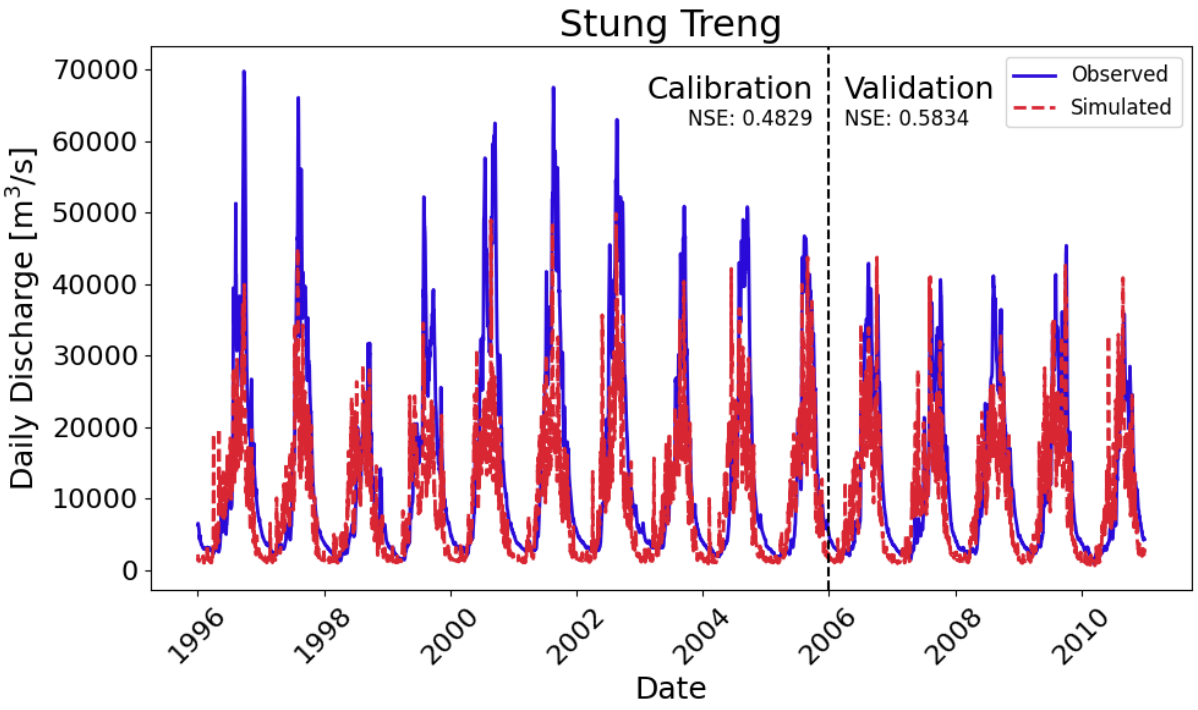

Figure 25: Observed and simulated hydrographs at Stung Treng

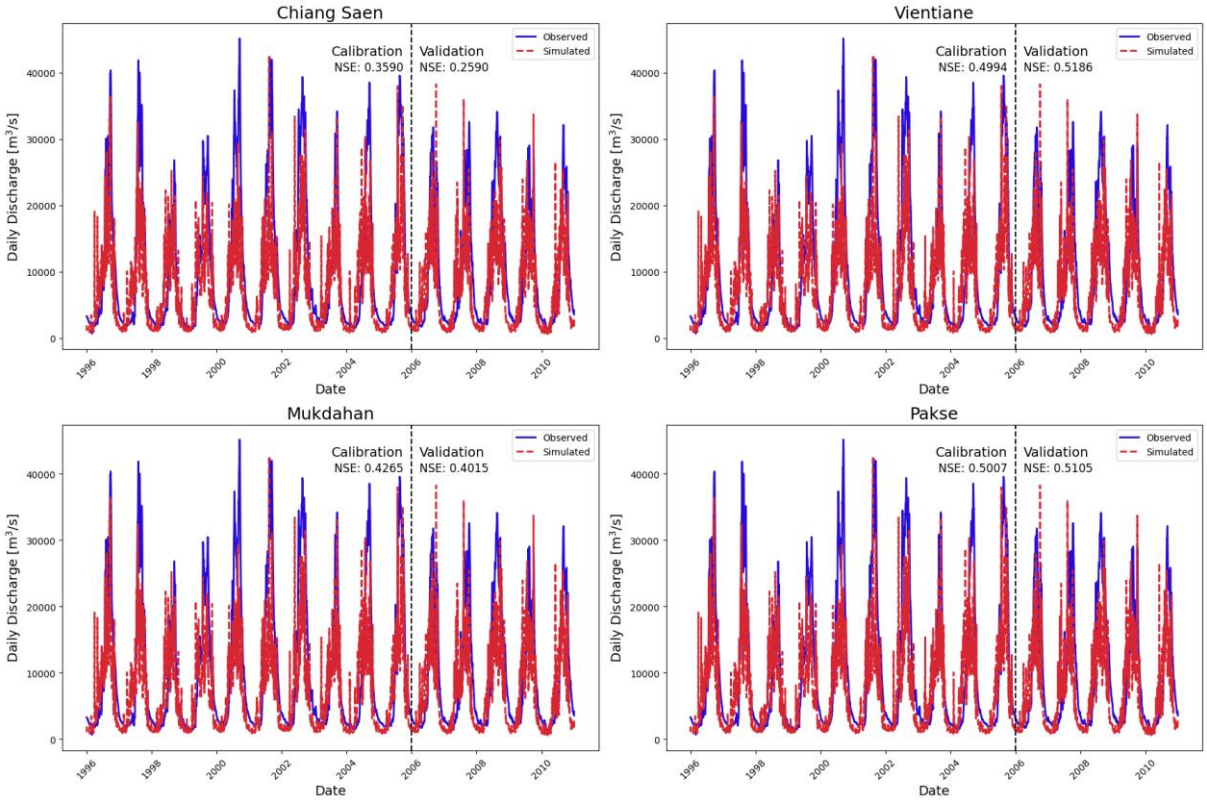

Figure 26: Observed and simulated hydrographs at Chiang Saen, Vientiane, Mukdahan, and Pakse

For the D-CASCADE model, we developed a preliminary dynamic version for the Mekong River. Once the calibration of VIC-Res is finalized, we will proceed with fully coupling the models following the outlined procedure.

In this initial version, we used a simplified river network of 179 reaches due to limited hydrological data. We began incorporating reservoirs and their trap efficiency, considering 73 dams (operational, under construction, and planned), which resulted in three distinct scenarios: a baseline with no dams (BAS), a scenario with operational and under-construction dams (DEF), and a full buildout scenario (FBO) that includes all planned dams. The model was calibrated using 20 years of hydrological data to simulate pre-dam sediment delivery to the Mekong Delta, historically 160 Mt/year.

Preliminary results indicate a significant reduction in sediment delivery, with a 27% decrease in the DEF scenario and 43% in the FBO scenario (Table 9). Upstream regions like the Lancang are increasingly cut off from delivery to the delta, leading to a shift in main contributors of delivered sediment from upstream to downstream provenance regions (Figure 27). This disconnection threatens the ecosystem integrity of the Mekong floodplains and delta, jeopardizing economic and food security and increasing risks like delta subsidence.

Table 9: Summary of results for the effect of sediment trapping on the amount of sediment delivered to the Mekong delta for all three scenarios

Scenarios	BAS	DEF	FBO
Name	Baseline	Definitive Future	Full build-out
Included Dams	none	Operational + under construction	DEF dams + planned dams
Sediment Delivery to he outlet (Mt/yr)	160.0	116.9	91.7
Difference to BAS	-	-26.9%	-42.7%

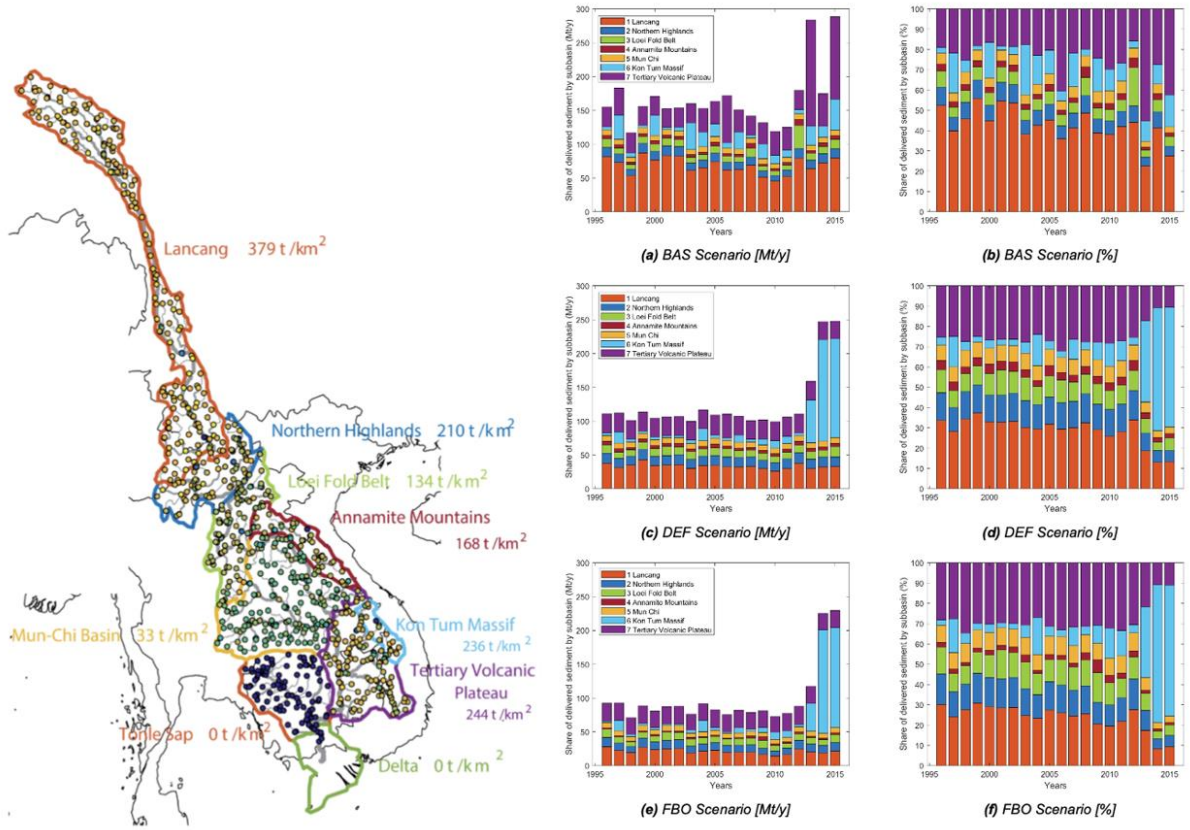

Figure 27 On the left panel we show the map of geomorphic regions shown in the same color scheme of the right panel and including their estimated annual sediment yields. On the right panel we illustrate the charts showing the average annual composition of the delivered sediment.

Once the calibration and validation of VIC-Res Mekong are finalized, we will use the simulated discharges from VIC-Res as the hydrological input for the dynamic version of CASCADE. This will allow us to reconstruct the sediment budget within the basin and to calibrate and validate D-CASCADE using the new dataset shown in the previous chapter.

Uncertainty and robustness are key aspects to consider when applying the IWMS framework for risk assessment, particularly in the context of future climate and hydrological changes. The VIC-Res model

describes the underlying physical processes of the hydrological cycle and water regulation through reservoirs. As such, it can reliably simulate system responses even under meteorological conditions that differ from the historical record, including future scenarios with unprecedented combinations of precipitation and temperature. Similar considerations apply to the D-CASCADE model, which, although conceptual in nature, has been designed to represent the main sediment sources, pathways, and sinks at basin scale.

Nevertheless, both models inherently involve uncertainties arising from parameterization and input data quality. In the context of SOS-Water, our framework acknowledges these limitations. Rather than aiming to provide precise daily predictions, the models are intended to capture basin-scale hydrological and sediment dynamics and to identify major spatial and temporal patterns relevant for management and policy decisions. At this scale, VIC-Res and D-CASCADE—both calibrated, validated, and widely applied in previous studies—offer a solid and practical basis for exploring alternative water and sediment management options.

Finally, a dedicated task in the final phase of the project will explicitly address model and scenario uncertainty, assessing their influence on the definition of the Safe Operating Space (SOS) for the Mekong River Basin under future climate and management scenarios.

Mekong Delta

The models are validated using time series data (water level, discharge, salinity, sediment load) at permanent hydrological stations and additional survey sites.

Result of model validation is evaluated using comparison of simulated and observed time series (charts in Figure 28, Figure 29, Figure 30) and statistical parameters (e.g. Nash Sutcliffe efficiency - NSE), maximum water level (values in table 10). Overall, there is very good evaluation of parameters across the entirety of the Mekong delta model domain (Table 10 and Table 11). For the validation against the flood period, the modelled results match the general trend of the flood flows in the period between May 2018 and February 2019 at the Tan Chau station. We do see that the model tends to smooth out the fluctuations of the system and tends to match the high peaks compared the lower values. We added a comparison between the model and the simulations at Tan Chau for a 5-month period between 01 July and 30 November. While our model misses some of the high and low values, we do see strong seasonality on the hourly time scale which demonstrates the validity of this model for the evaluation of water availability in the Mekong.

The comparison chart of the conformity of the measured and simulated water level and flow value series at many locations shows the model's ability to calculate well the fluctuations in amplitude and phase of tides, the flow distribution on river branches and canals under long-term changing terrain conditions and short-term regulation of water works.

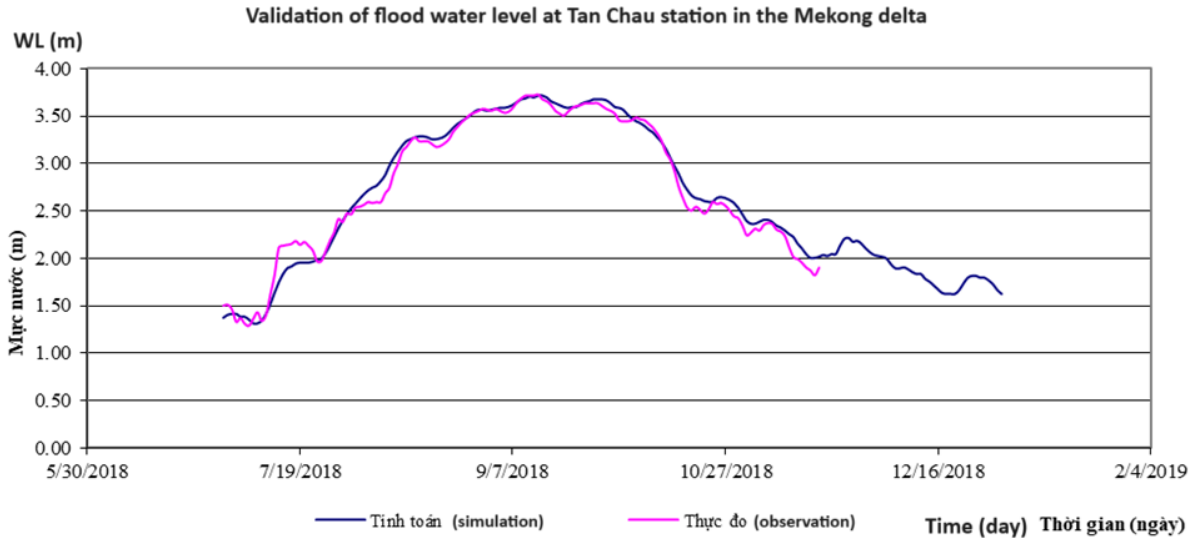

Figure 28: Validation of VRSAP model for flood flow water level (1 July to 30 November) at upper station (Tan Chau)

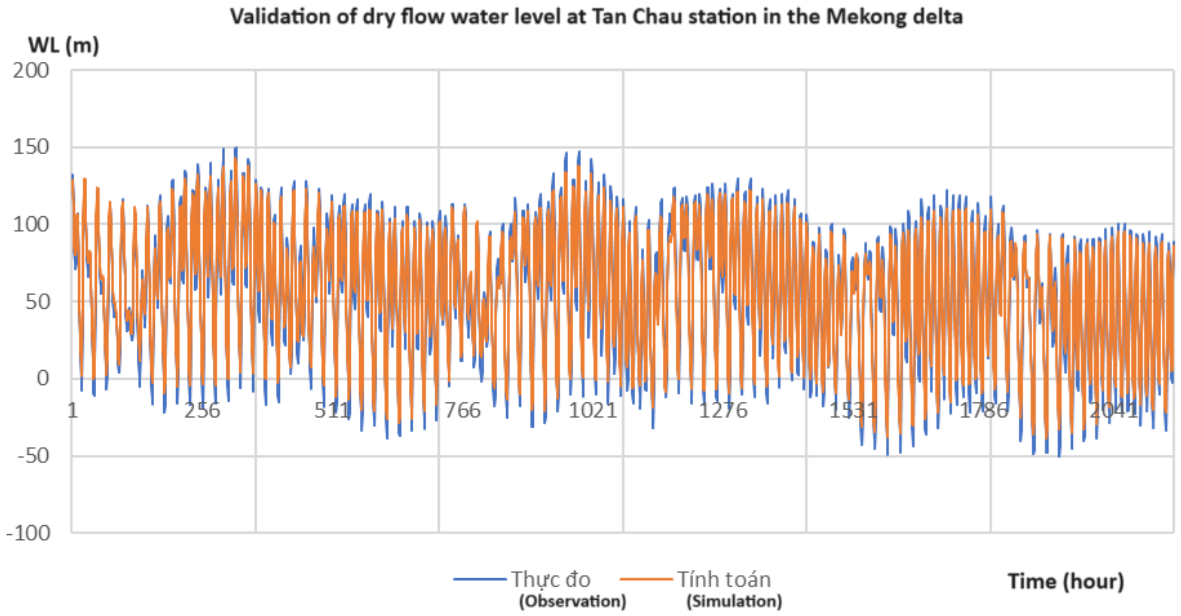

Figure 29: Validation of VRSAP model for dry flow water level (1 February to 30 April) at upper station (Tan Chau)

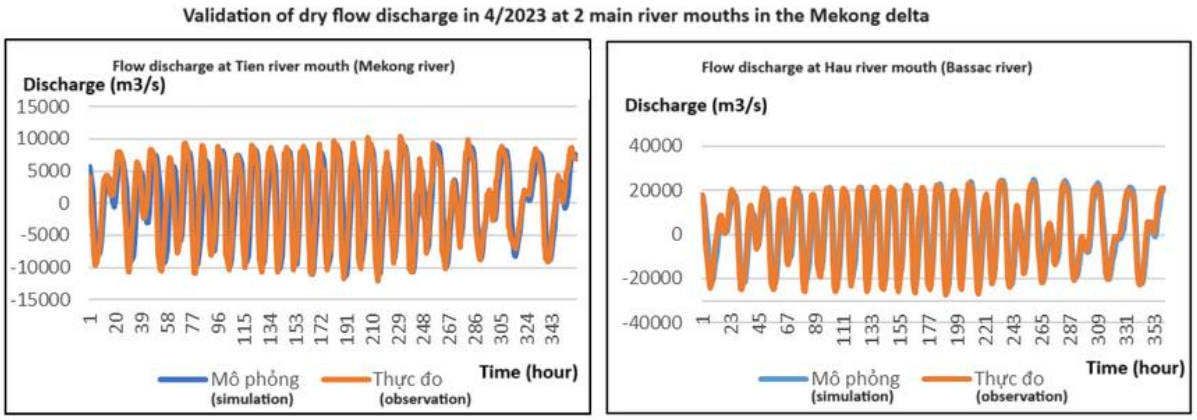

Figure 30: Validation of VRSAP model for dry flow discharge at main river mouth

Table 10: VSARP model validation for flood water level in 2011 using statistical parameters and comparison of maximum value

Station name	Hmax_obs (m)	Hmax_sim (m)	NSE ()	RSR ()	Evaluation
Tân Châu	4,86	4,69	0,98	0,06	Very good
Châu Đốc	4,27	4,22	0,97	0,07	Very good
Vàm Nao	3,60	3,56	0,97	0,06	Very good
Chợ Mới	3,49	3,41	0,97	0,06	Very good
Cao Lãnh	2,57	2,67	0,91	0,09	Very good
Mỹ Thuận	2,03	2,22	0,84	0,26	Very good
Chợ Lạch	1,96	2,01	0,87	0,34	Very good
Mỹ Tho	1,78	1,75	0,90	0,30	Very good
Hòa Bình	1,66	1,65	0,84	0,32	Very good
Long Xuyên	2,81	2,83	0,87	0,10	Very good
Cần Thơ	2,15	2,18	0,78	0,24	Very good
Đại Ngãi	2,14	1,92	0,76	0,47	Very good
Mỹ Hóa	1,73	1,77	0,89	0,32	Very good
Trà Vinh	1,82	1,85	0,86	0,34	Very good
Mộc Hóa	2,80	2,77	0,98	0,07	Very good
Tuyên Nhơn	1,95	1,92	0,93	0,14	Very good
Tân An	1,72	1,59	0,60	0,63	Good
Bến Lức	1,51	1,46	0,82	0,41	Very good
Hưng Thạnh	3,27	3,21	0,98	0,08	Very good
Kiến Bình	2,24	2,15	0,96	0,10	Very good
Cai Lậy	1,87	2,03	0,91	0,11	Very good
Long Định	1,55	1,6	0,87	0,31	Very good
Xuân Tô	4,47	4,25	0,99	0,06	Very good
Tri Tôn	2,76	2,77	0,97	0,08	Very good

Tân Hiệp	1,38	1,5	0,90	0,14	Very good
Vị Thanh	0,74	0,79	0,63	0,25	Good
Phụng Hiệp	1,58	1,62	0,81	0,25	Very good
Phước Long	0,69	0,71	0,63	0,66	Good
Cà Mau	0,75	0,86	0,60	0,29	Good
Năm Căn	1,56	1,5	0,86	0,37	Very good

Table 11: Depicts the evaluation level for the RSR and NSE shown in Table 10

Evaluation level	RSR	NSE
Very good	$0,00 \leq RSR \leq 0,50$	$0,75 \leq NSE \leq 1,00$
Good	$0,50 \leq RSR \leq 0,60$	$0,65 \leq NSE \leq 0,75$
Aceptable	$0,60 \leq RSR \leq 0,70$	$0,50 \leq NSE \leq 0,65$

Rhine

To evaluate the updated reservoir scheme in the Rhine basin, we first evaluated its impact on discharge by calculating the monthly discharge between the GRDC stations in the Rhine and our five models (Figure 31). We used the monthly KGE values and plotted cumulative distribution functions for the Baseline (black), BaseGeoDAR (grey), and all of the data-derived operations with the different command areas (250, 600, and 1100 in shades of pink). While we don't see any large differences between the different command areas (suggesting that we can simply focus on the evaluation of one command areas: 250), we do see slight differences between the operational schemes. The data-derived operations have 35% of their values between –0.5 and –0.75 while the generic operations have only 34% which shows a negative impact on the streamflow regimes. This increase in negative KGE values potentially comes from the downstream impact of reservoir operations. That said, all models have 20% of their values greater than 0.5 which suggests there is a decrease in performance

around 0 as the data-derived operations have slightly lower values here.

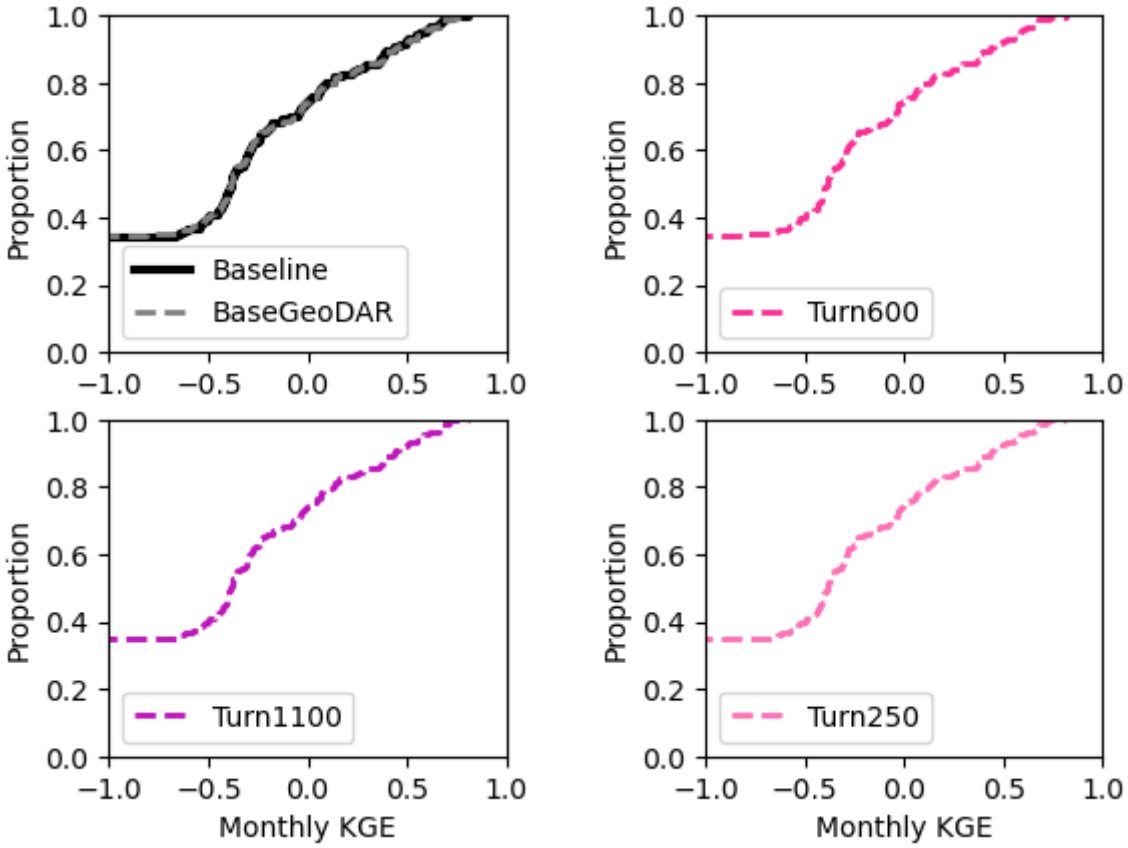

Figure 31: Cumulative density plot of the monthly KGE values in the Rhine basin. Lines are colored by the model used. Baseline and BaseGeoDAR use the same generic reservoir operations derived from van Beek et al., 2011 and other differ by the input map (GRanD Bas Baseline and GeoDAR for BaseGeoDAR). The pink lines denote the data-derived operations for a variety of command areas.

To further dive into the differences between the two reservoir models (i.e. generic vs. data-derived operations), we also compared the two reservoirs schemes with the GeoDAR base map (vanBeekGeo and Turn250) with the baseline operations. This allows us to look at the difference in the operational schemes without having to account for variations in input maps. In Figure 31 we plot these relative differences as density plots for the three main components of KGE: correlation (Figure 31a) bias ratio (Figure 31, b) and the variability ratio (Figure 31, c). Both the variability and bias ratios do not vary between the models, meaning there is no significant difference between the operational schemes for these two components. For correlations, we do see a slight difference. The vanBeekGeo model with the updated GeoDAR map and the generic operations has slightly more positive correlations with the GRDC stations. This suggests that the generic operations are slightly more accurate than the data-derived ones along the Rhine River.

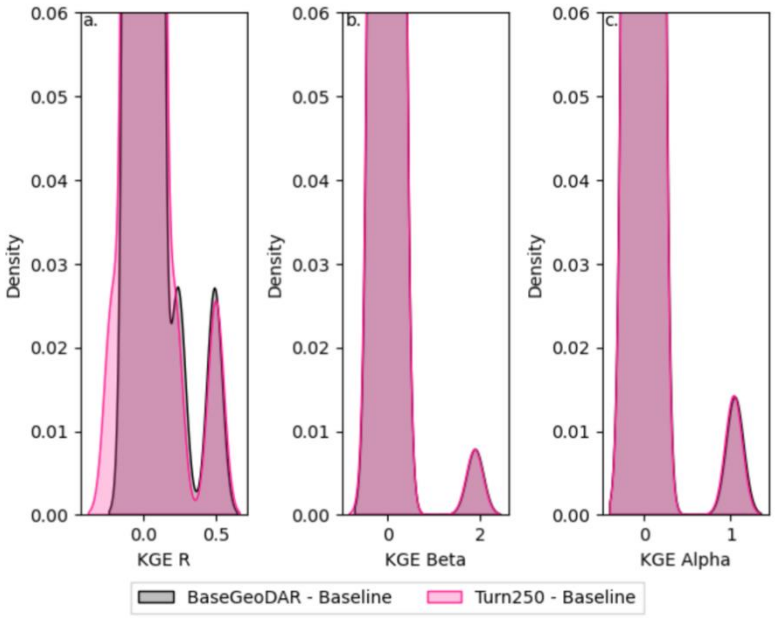

Figure 32: Panel plot of the difference between the Turn250 and BaseGeoDAR models and the Baseline model for the three components of KGE: correlation (a), bias ratio (b), and variance ratio (c).

In order to better highlight the periods where the operations are different from the observations, we opted to plot discharge timeseries at the most downstream point along the Rhine (Lobith, NL) during the 2018 drought and a normal year (i.e. 1999, Figure 33) and flow duration curves at three main points along the Rhine: Lobith, NL for the lower Rhine; Andernach, DE for the middle Rhine; and Basel Rheinhall, CH for the upper Rhine. During a normal year (Figure 32) we see that all models have the same general trends as the observations and in fact do align fairly well during the winter and spring. That said, PCRGLOBWB 2 has a tendency to overestimate the amount of water at Lobith during the late spring and summer months. During a dry year (Figure 33), we observe that the overall trends are accurate, yet the PCRGLOBWB2.0 discharge is much higher compared to the discharge at Lobith during the summer. From the FDC curves (Figure 34) we observe that the Turn250 model is higher in the headwaters in Basel Rheinhalle, CH (shown by the high values with a 0-exceedance probability). We also observe that the FDCs become shallower for the observations in the middle (Andernach, DE) and lower (Lobith, NL) basins. This suggests that the impact of regulation and water extractions within the Rhine is more pronounced in PCRGLOWBW 2.

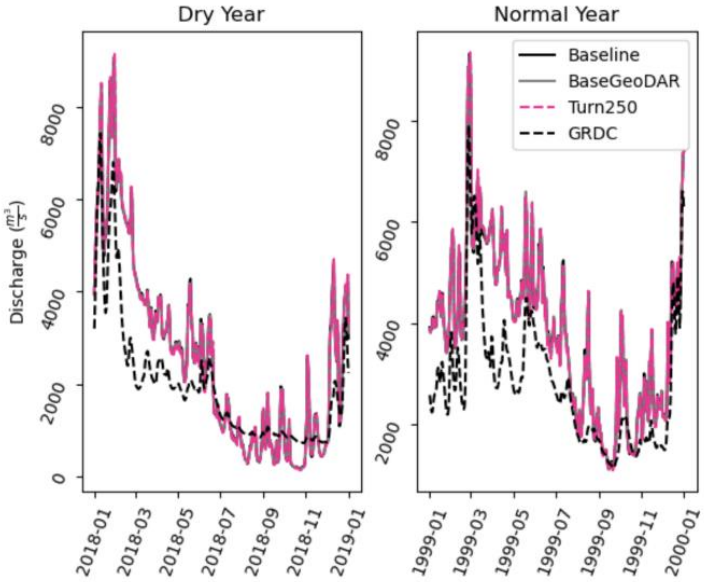

Figure 33: Line plot showing the different models: Turn250 (pink), BaseGeoDAR (grey) and Baseline (black) against GRDC observations (dashed black) at Lobith, NL for a dry year (a) and a normal year (b).

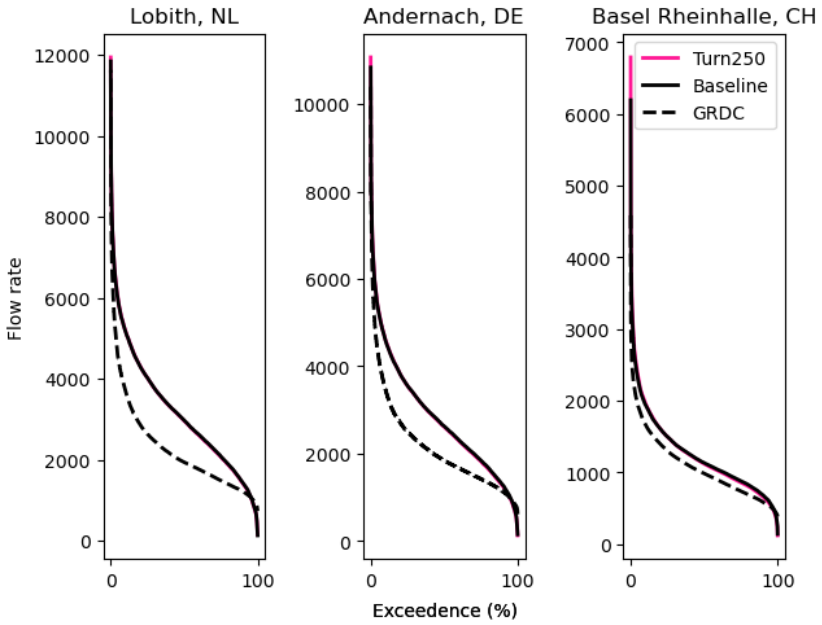

Figure 34: Flow duration curves (FDC) for all three models: Turn250 (pink), BaseGeoDAR (grey) and Baseline (black) and GRDC observations (black dashed), at three locations along the Rhine (Lobith, NL for the lower Rhine, Andernach, DE for the middle Rhine, and Basel Rheinhalle, CH for the upper Rhine).

While the streamflow KGE and KGE components and the FDCs did not show strong improvements between the models, plotting the long term average monthly reservoir storage fraction over time showed more accurate storage levels (Figure 35). The Turn250 run has a RMSE of 0.05 while the Baseline and BaseGeoDAR have RMSE values of 0.09 and 0.12 respectively. In terms of average storage fraction and trends, the Turn250 model is more aligned with the remotely sensed observations suggesting that while the updated scheme does not increase the streamflow performance it does

increase the storage performance. In order to further improve the model performance in the Rhine basin, it would be useful to have more direct observations of reservoir storage levels with which to calibrate our reservoir scheme. The Rhine basin, while having hundreds of reservoirs, has gaps in coverage of the remotely sensed reservoir data from GloLakes due to the high latitudes and high occurrence of cloudy days. Increasing the number of direct observations would enhance the performance of PCR-GLOBWB2 with respect to both the reservoir dynamics as well as the streamflow.

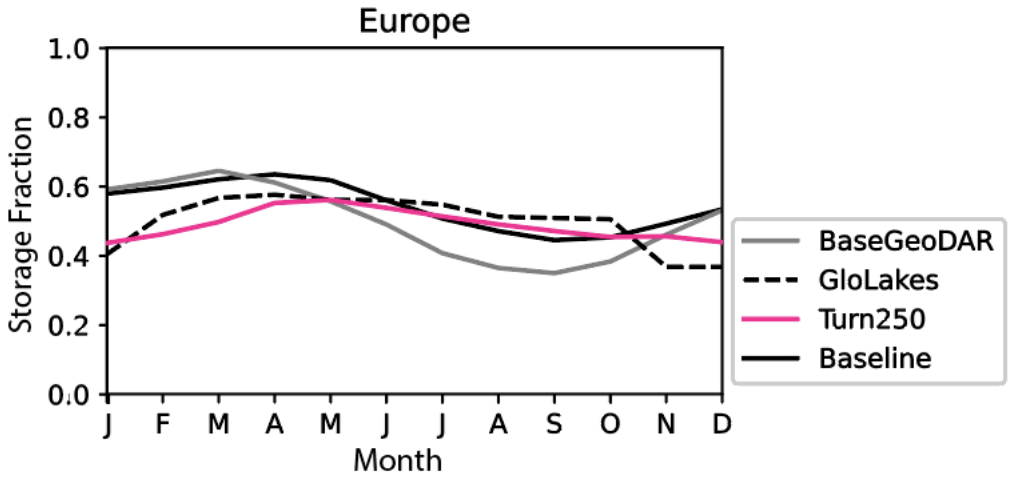

Figure 35 Depicts the long term average monthly reservoir storage fraction across the European continent for three model runs (Baseline in black, BaseGeoDAR in grey, and Turn250 in pink). We also included the longterm monthly reservoirstorage fraction from a remotely sensed dataset: GloLakes in black dashed lines.

Lastly, we looked at the impact of our modelling framework on total water storage (Figure 37) and reservoir storage (Figure 36). We compared our total water storage variables with the liquid water equivalent from the combined GRACE-FO product. While this is not a direct comparison, it does allow us to evaluate trends. We observe that total water storage from our models follow the increasing trend of GRACE–FO from 2022–2023, supporting the models' validity. To further evaluate the impact of our reservoir operations, we compared the long-term seasonal modeled reservoir storage to the long-term seasonal storage from the GloLAKES dataset (a dataset of remotely sensed reservoir storage timeseries from 1984–2022). Initially, we observe that the data-derived reservoir operations (in pink) contain much lower storage average when compared with the generic reservoir scheme (black and grey). This is due in part to 1) the more condensed operational bounds in the data-derived scheme (between 20% to 75% of capacity depending on the reservoir) than the generic operational bounds (between 10% and 75% of capacity), and 2) an increase in releases to meet demand in the dataderived scheme. We also see that the data-derived operations are more accurate than the baseline operations (RMSE of 0.17 for the Baseline model and 0.1 for the data-derived operations defined as Turn250). Finally, we also observe that the data-derived operations follow the observed reservoir storage trends (i.e., high storage in the summer and autumn, with lower storage in winter and increasing storage in the spring). Ultimately, our results from the discharge and the storage validation show that our updated reservoir scheme does not lead to large differences in the discharge dynamics or values but does improve the reservoir storage and therefore contains a more accurate depiction of water availability.

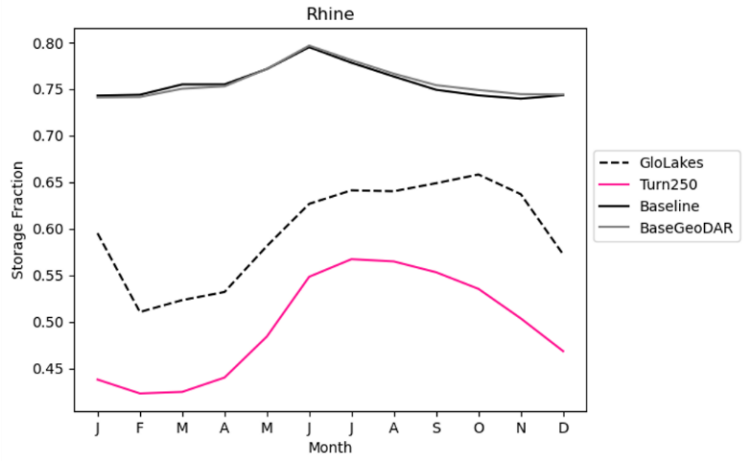

Figure 36: Depicts long term montlhy average reservoir storage fraction in the Rhine basin for all three models: Turn250 in pink, BaseGeoDAR in grey, and Baseline in black, against modelled values in GloLakes (dashed black) (Hou et al., 2024).

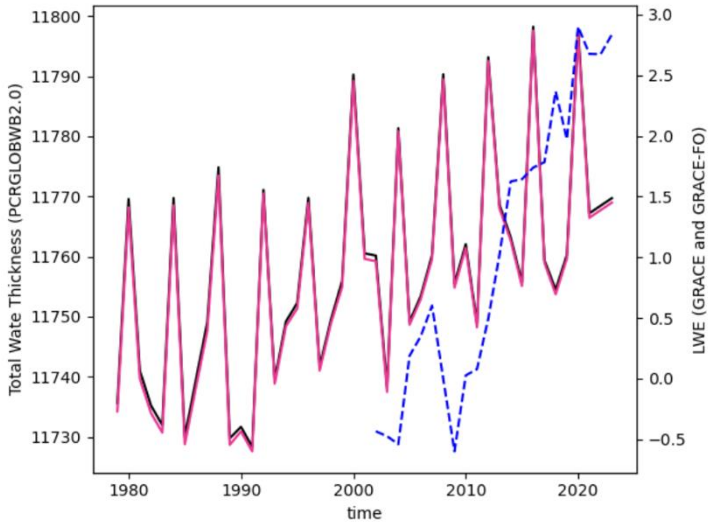

Figure 37: Depicts the annual total water storage in the Rhine basin for the Turn250 (pink) and the Baseline (black) models on the left axis. The right axis depicts the liquid water equivalent (LWE) in GRACE-FO in dashed blue.

In summary, the calibration of PCR_GLOBWB2 demonstrates that the hydrologic outputs are sufficient for the calculation of a basin scale SOS. This is primarily due to the increase in accuracy for our reservoir storages that provide a more realistic estimation of how much water is stored there. Additionally, our calibration of the two main land cover types ensures that we are not extracting more water for evaporative demands and can provide a more holistic evaluation of the water available for multiple uses. As with any modelling setup, there are points for improvement such as :

1. Moving from static reservoir operations (i.e., keeping the same reservoir operations for each year instead of changing them yearly or with other operational changes) could enhance the predictions of available water for withdrawals
2. Increasing the resolution of the land cover type in the PCR-GLOBWB2 model could lead to more accurate predictions of the green water demands (i,e., soil moisture, an PET)

In the same way as the Danube, Jucar and Mekong, the Rhine addresses uncertainty through the use of ISIMIP3b climate change scenarios and models. Using the same climate scenarios and adaptations (discussed more in later deliverables) ensures coherency in the SOS project story lines. The robustness of PCR-GLOBWB2 to these general circulation models and climate scenarios has been demonstrated in other projects (i.e. ISIMIP). Additionally, in our calibration, we ensured that we performed calibration with observed climate inputs (W5E5) as well as a selection of the global circulation models to ensure that the model setup was as robust as possible to potential changes.

Biodiversity Modelling: Initial model predictions

We present the initial SDM predictions, developed using the Random Forest machine learning algorithm for each case study and a subset of the species. The models depict the potential habitat suitability of the species and consist of a steppingstone towards addressing the environmental tolerances of single species against changing environmental conditions, such as increasing temperatures, changing precipitation patterns and increases in water abstraction.

Examples of habitat suitability predictions for the Danube basin

For the Danube basin the initial round of habitat suitability predictions were done for 58 species. The maps are being uploaded to the IGB Geonode visualization tool and can be consulted here: (https://geo.igb-berlin.de/maps/953). Below are examples of four species with contrasting distribution patterns through the Danube basin. Attached to each map is a zoom-in of particular regions to visualize in more detail the local patterns of habitat suitability along the stream network (Figure 38).

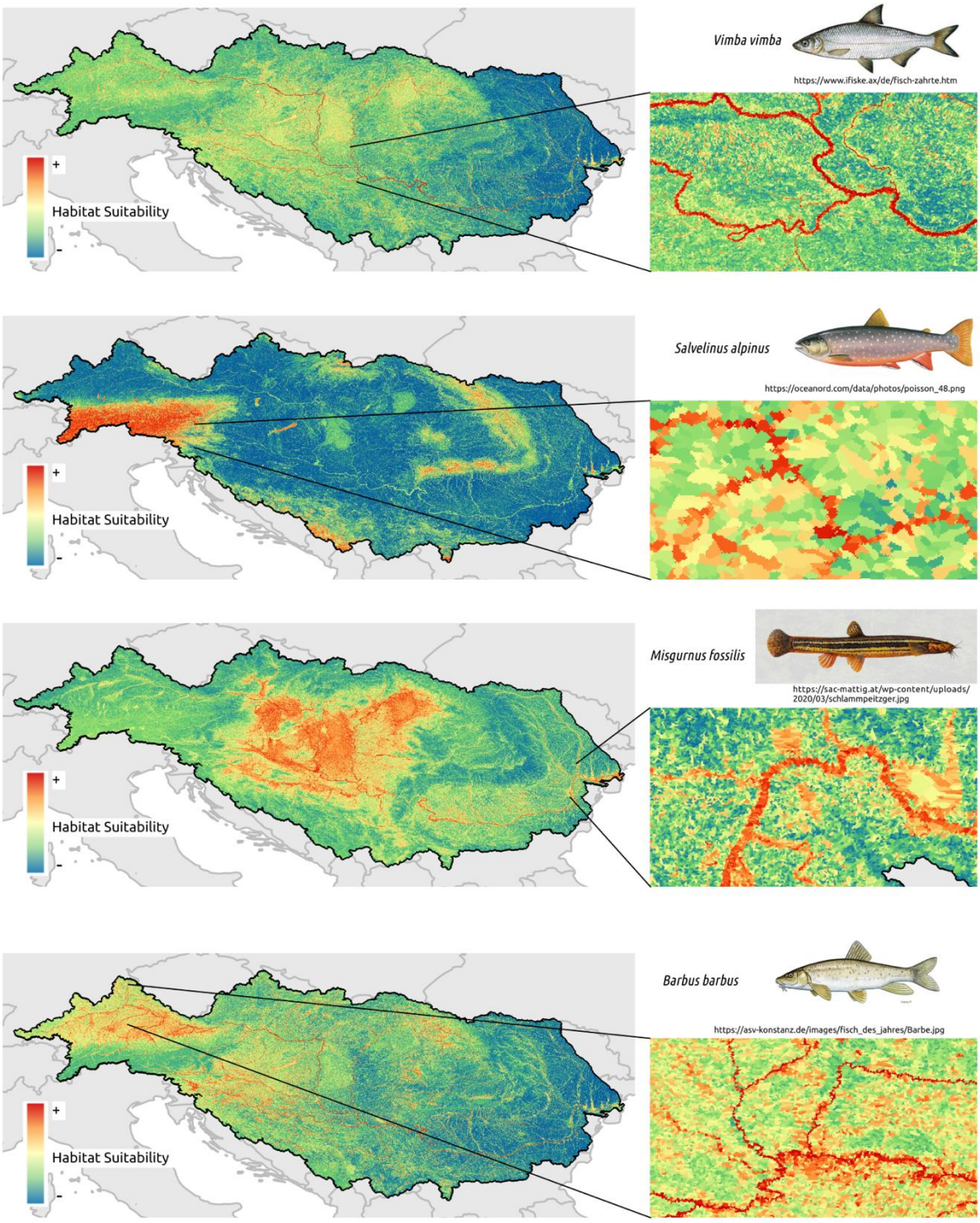

Figure 38: Habitat suitability maps for four species in the Danube Basin, all of them having different habitat suitability distribution patterns along the river network.

Examples of habitat suitability predictions for the Júcar basin

For the Júcar basin the suitable habitat of 35 species were initially modeled. The maps are being uploaded to the IGB Geonode visualization tool and can be consulted here: (https://geo.igb-berlin.de/maps/951). The examples below illustrate contrasting distribution patterns of four different

species (Figure 39). The habitat suitability probabilities for all 35 species can be summed up to obtain a description of the richness patterns of habitat suitability in the entire basin (Figure 40).

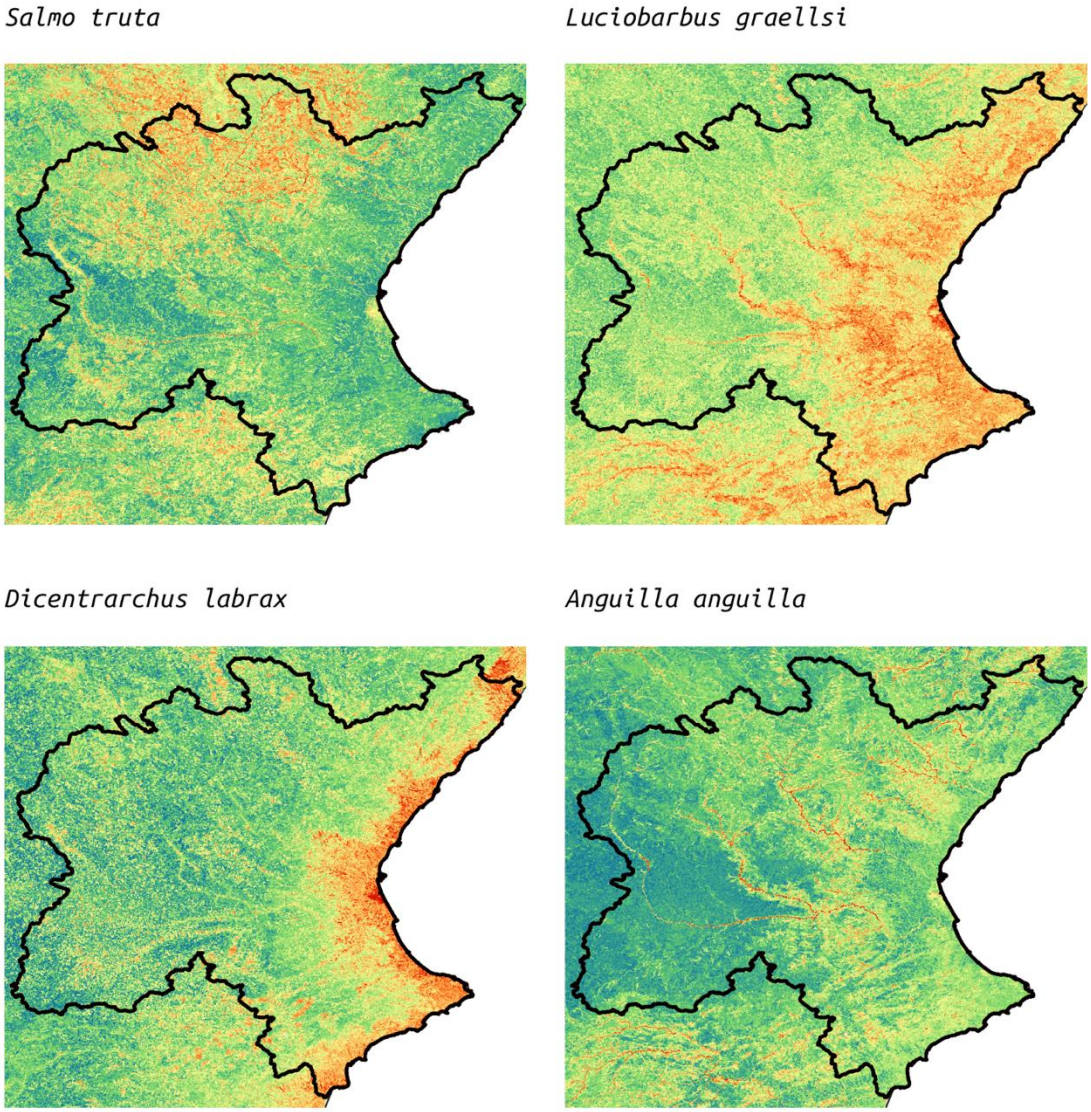

Figure 39: Habitat suitability maps for four species in the Júcar Basin, all of them having different habitat suitability distribution patterns along the river network. The color gradient represents habitat suitability values, where red colors are high suitabilit

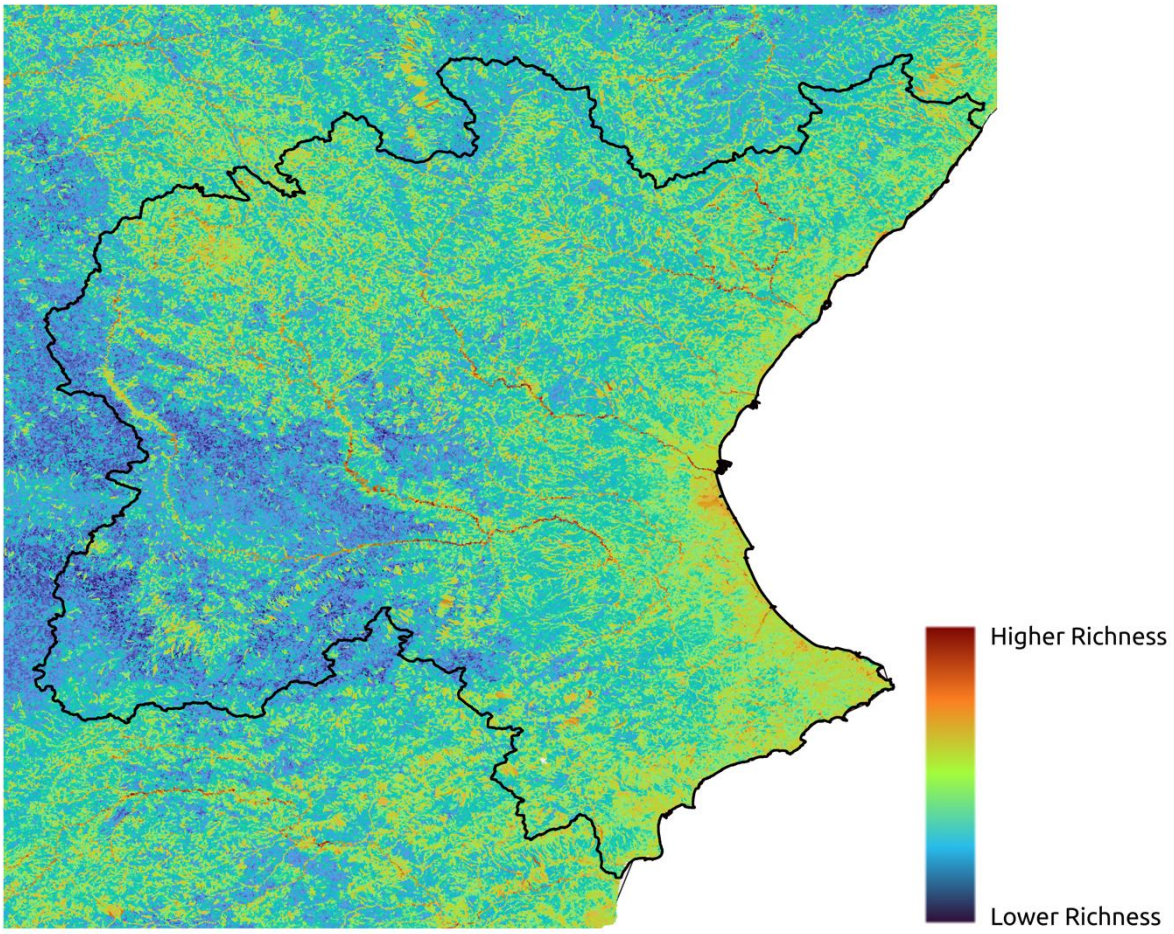

Figure 40: Geographical patterns of species habitat richness, understanding high richness areas (i.e., dark red colors) as areas where high suitability values were found for most species analyzed.

Examples of habitat suitability predictions for the Rhine basin

Initial habitat suitability predictions of 27 species were done for the Rhine basin. The maps are being uploaded to the IGB Geonode visualization tool and can be consulted here: (https://geo.igb-berlin.de/maps/957). Figures 41 and 42 illustrates the habitat suitability distribution patterns along the basin for four different species showing distinct patterns of habitat suitability.

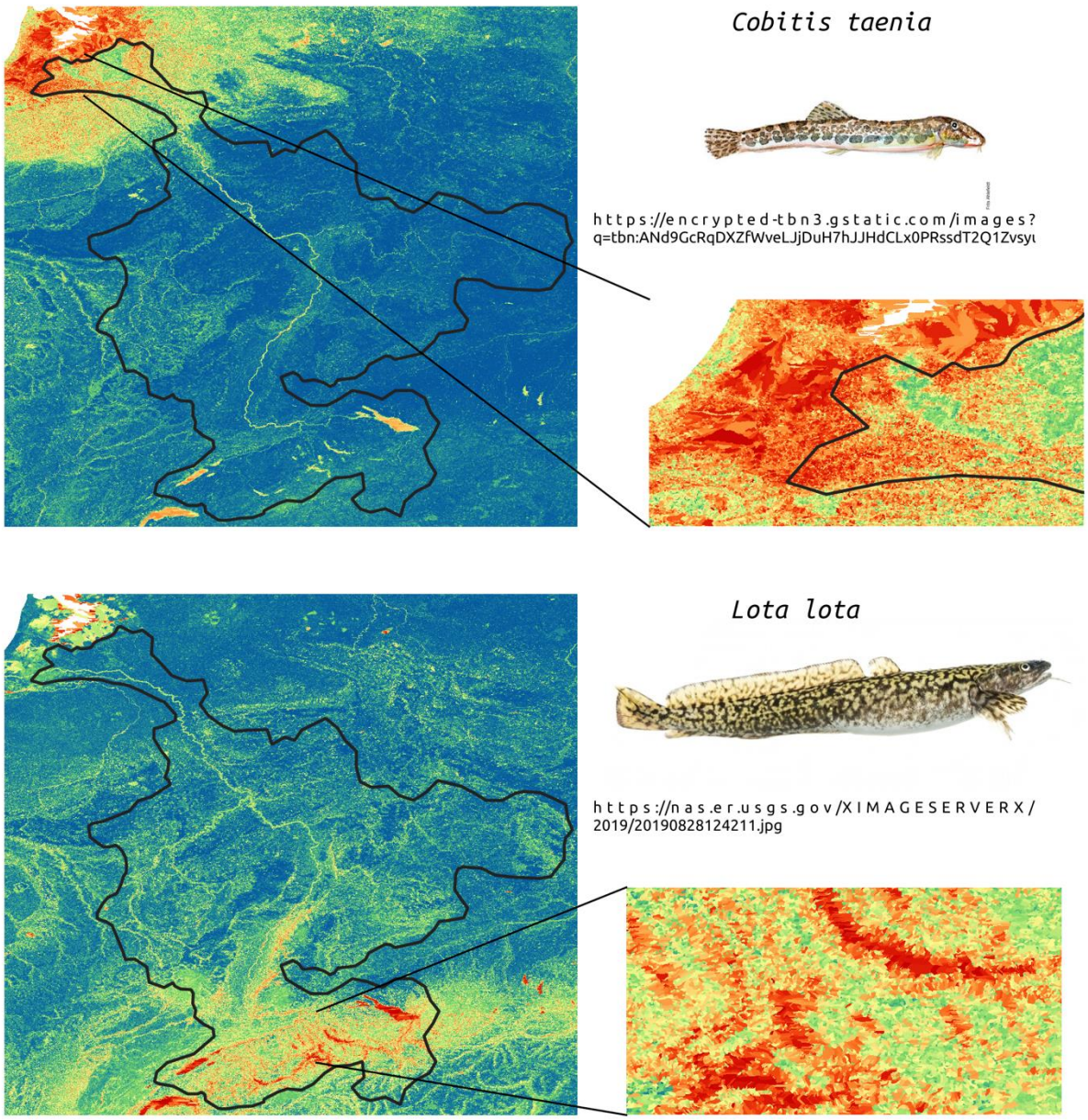

Figure 41: Habitat suitability maps for four species in the Rhine Basin, all of them having different habitat suitability distribution patterns along the river network. The color gradient represents habitat suitability values, where red colors are high suitability and blue colors low suitability

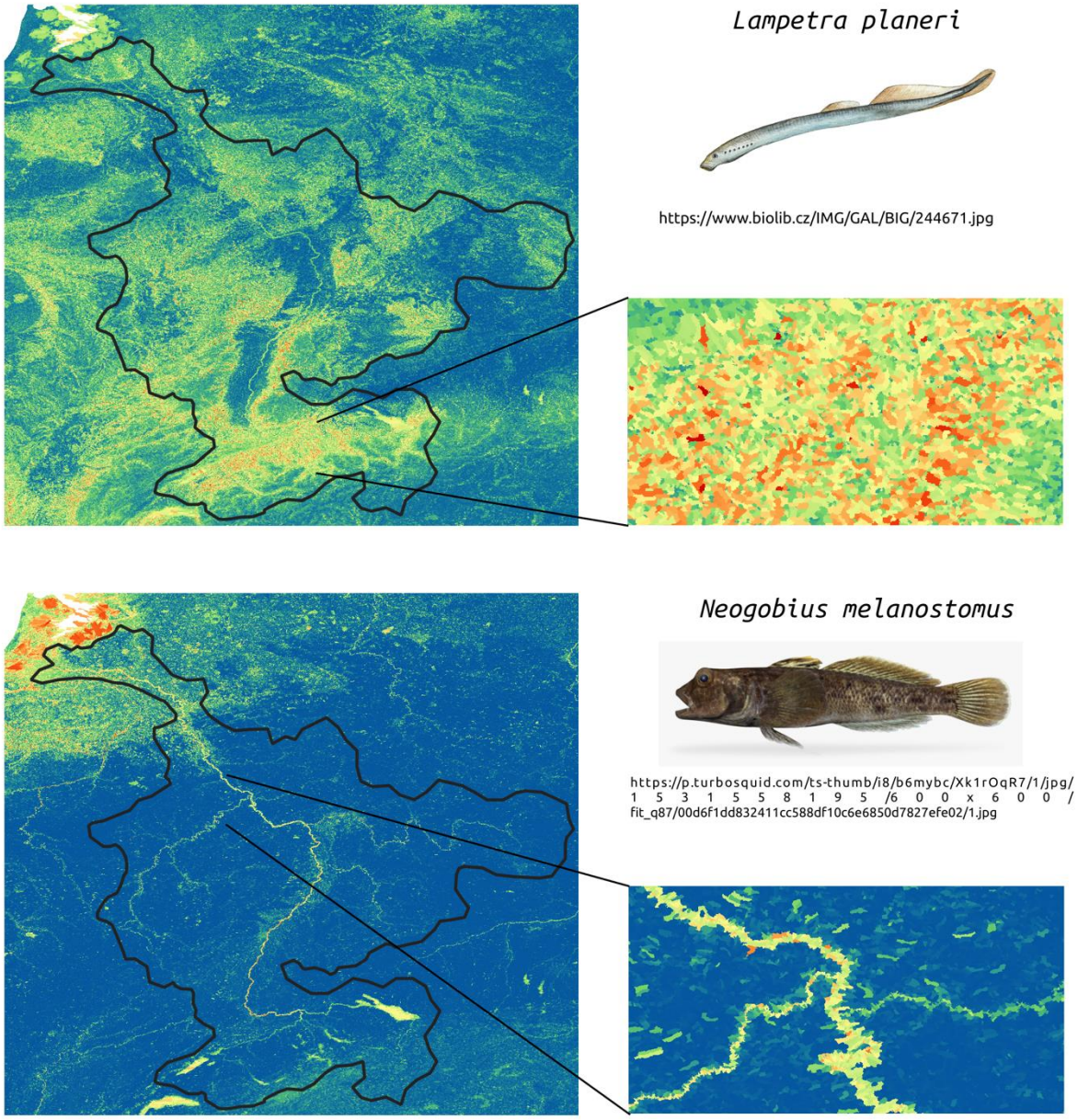

Figure 42: Habitat suitability maps for four species in the Rhine Basin, all of them having different habitat suitability distribution patterns along the river network. The color gradient represents habitat suitability values, where red colors are high suitability and blue colors low suitability

Examples of habitat suitability predictions for the Mekong basin

The initial search for fish occurrence data for the Mekong basin found a total of 941 species. However, the next step of quality check and relevance for the project will reduce the number of species that will be modeled. Initial habitat suitability models were applied for 27 species. The maps are being uploaded to the IGB Geonode visualization tool and can be consulted here: (https://geo.igb-berlin.de/maps/955). The map of three species as an example can be seen in Figure 43.

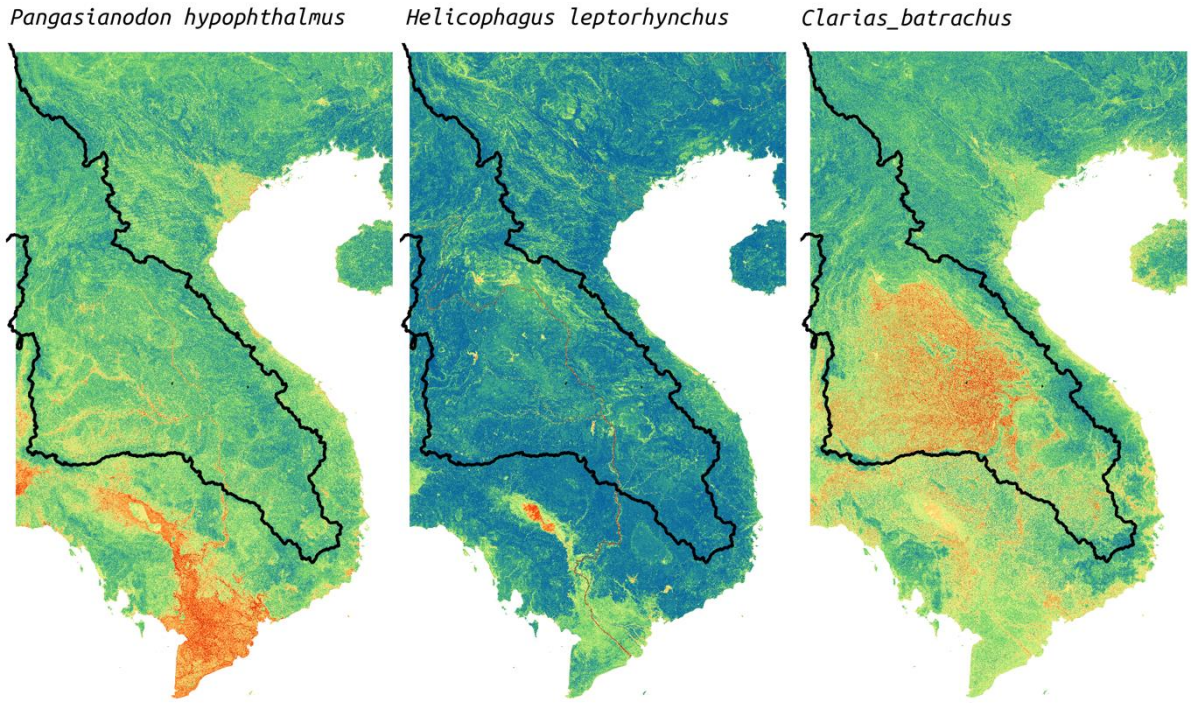

Figure 43: Habitat suitability maps for three species in the southern section of the Mekong Basin, all of them having different habitat suitability distribution patterns along the river network. The color gradient represents habitat suitability values, where red colors are high suitability and blue colors low suitability.

Conclusions

The main objective of this deliverable is to establish linkages between Water System Models and Impact Models and building and benchmarking Integrated Water Modeling Systems.

The results show that improvements have been made to the models in terms of reservoir representation and the quantification of the evapotranspiration flux, which lead to small improvements in the discharge estimates for the Rhine and Danube. There is also work in progress to improve glaciers and snowmelt dynamics. The ability of the water system models to better capture important processes like evapotranspiration and the reservoir storage is also hypothesized to positively reflect on their ability to capture the impact of future climate change and the human-water interactions.

In the Jucar case study basin, we find that coupling a hydro-economic model with a hydrological model can accurately estimate irrigation gifts in several regions in the Jucar basin as well predict the remaining discharge to the sea.

The impact assessment for the Mekong shows that by coupling hydrological model, reservoir expansion scenarios and the D-CASCADE model, sediment loads of the river can be decreased by 27 to 43%. The construction of dams will trap sediment which in turn will have an impact on the floodplain and delta development that in part depend on this sediment transport from upstream regions.

Regarding the impact models, we find interesting spatial patterns when it comes to the distribution and suitability of fish species to survive in different parts of the case study basins. For the Danube we were able to simulate the habitat suitability for 58 species, while the Jucar (35), Rhine (25) and Mekong (27) have slightly lower numbers of modelled fish species included in the ecosystem modelling. For the Mekong, this is mostly the result of reduced data quality, while the known abundance of species in these regions is very high.

These results show that we can consistently link hydrological with impact models, either in an offline coupling, hydrology feeding into the impact model without feedbacks to the hydrological system (e.g., biodiversity modelling) or an online coupling (e.g., hydro-economic modelling) where the impact model also has a direct impact on the hydrological fluxes.

Overall, we found that the performance of the different WSMs and IMS is satisfactory and provides a good benchmark to be used within the SOS-Water project for future modelling simulations.

References

Amatulli, G., Garcia Marquez, J., Sethi, T., Kiesel, J., Grigoropoulou, A., Üblacker, M. M., Shen, L. Q., & Domisch, S. (2022). Hydrography90m: A new high-resolution global hydrographic dataset. Earth System Science Data, 14(10), 4525–4550. https://doi.org/10.5194/essd-14-4525-2022

Ang, W. J., Park, E., Pokhrel, Y., Tran, D. D., & Loc, H. H. (2024). Dams in the Mekong: A comprehensive database, spatiotemporal distribution, and hydropower potentials. Earth System Science Data, 16(3), 1209–1228. https://doi.org/10.5194/essd-16-1209-2024

Biemans, H., Haddeland, I., Kabat, P., Ludwig, F., Hutjes, R. W. A., Heinke, J., von Bloh, W., & Gerten, D. (2011). Impact of reservoirs on river discharge and irrigation water supply during the 20th century. Water Resources Research, 47(3). https://doi.org/10.1029/2009WR008929

Burek, P., Satoh, Y., Kahil, T., Tang, T., Greve, P., Smilovic, M., Guillaumot, L., Zhao, F., & Wada, Y. (2020). Development of the Community Water Model (CWatM v1.04) – a high-resolution hydrological model for global and regional assessment of integrated water resources management. Geoscientific Model Development, 13(7), 3267–3298. https://doi.org/10.5194/gmd-13-3267-2020

Chua, S. D. X., & Lu, X. X. (2022). Sediment load crisis in the Mekong River Basin: Severe reductions over the decades. Geomorphology, 419, 108484. https://doi.org/10.1016/j.geomorph.2022.108484

CHJ (2023). Plan Hidrológico de la demarcación hidrográfica del Júcar. Ciclo de planificación hidrológica 2022-2027. Memoria (in Spanish).

Dang, T. D., Vu, D. T., Chowdhury, A. F. M. K., & Galelli, S. (2020). A software package for the representation and optimization of water reservoir operations in the VIC hydrological model. Environmental Modelling & Software, 126, 104673. https://doi.org/10.1016/j.envsoft.2020.104673

Elith, J., & Leathwick, J. R. (2009). Species Distribution Models: Ecological Explanation and Prediction Across Space and Time. In Annual Review of Ecology, Evolution, and Systematics (Vol. 40, Issue Volume 40, 2009, pp. 677–697). Annual Reviews. https://doi.org/10.1146/annurev.ecolsys.110308.120159

Engelund, F. and Hansen, E. (1967), A monograph on sediment transport in alluvial streams. Technical University of Denmark. https://repository.tudelft.nl/record/uuid:81101b08-04b5-4082-9121-861949c336c9

FAO (2012) Crop yield response to water. Food and Agriculture Organization of the United Nations. https://www.fao.org/3/i2800e/i2800e.pdf

Funk, C., Peterson, P., Landsfeld, M., Pedreros, D., Verdin, J., Shukla, S., Husak, G., Rowland, J., Harrison, L., Hoell, A., & Michaelsen, J. (2015). The climate hazards infrared precipitation with stations--a new environmental record for monitoring extremes. Scientific data, 2, 150066. https://doi.org/10.1038/sdata.2015.66

Gan, R., Zhang, Y., Shi, H., Yang, Y., Eamus, D., Cheng, L., Chiew, F. H. S., & Yu, Q. (2018). Use of satellite leaf area index estimating evapotranspiration and gross assimilation for Australian ecosystems. Ecohydrology, 11(5), e1974. https://doi.org/10.1002/eco.1974

Gill, M. A. (1979). Sedimentation and useful life of reservoirs. Journal of Hydrology, 44(1), 89–95. https://doi.org/10.1016/0022-1694(79)90148-3

Hanasaki, N., Kanae, S., Oki, T., Masuda, K., Motoya, K., Shirakawa, N., Shen, Y., & Tanaka, K. (2008). An integrated model for the assessment of global water resources – Part 1: Model description and input meteorological forcing. Hydrology and Earth System Sciences, 12(4), 1007–1025. https://doi.org/10.5194/hess-12-1007-2008

Hoch, J. M., Sutanudjaja, E. H., Wanders, N., Van Beek, R. L. P. H., & Bierkens, M. F. P. (2023). Hyper-resolution PCR-GLOBWB: Opportunities and challenges from refining model spatial resolution to 1 km over the European continent. Hydrology and Earth System Sciences, 27(6), 1383–1401. https://doi.org/10.5194/hess-27-1383-2023

Hou, J., Van Dijk, A. I. J. M., Renzullo, L. J., & Larraondo, P. R. (2024). GloLakes: Water storage dynamics for 27\,000 lakes globally from 1984 to present derived from satellite altimetry and optical imaging. Earth System Science Data, 16(1), 201–218. https://doi.org/10.5194/essd-16-201-2024

Kahil, M. T., Ward, F. A., Albiac, J., Eggleston, J., & Sanz, D. (2016). Hydro-economic modeling with aquifer-river interactions to guide sustainable basin management. Journal of Hydrology, 539. https://doi.org/10.1016/j.jhydrol.2016.05.057

Kittel, C. M. M., Jiang, L., Tøttrup, C., & Bauer-Gottwein, P. (2021). Sentinel-3 radar altimetry for river monitoring – a catchment-scale evaluation of satellite water surface elevation from Sentinel-3A and Sentinel-3B. Hydrology and Earth System Sciences, 25(1), 333–357. https://doi.org/10.5194/hess-25-333-2021

Koehnken, L, (2014). Discharge Sediment Monitoring Project DSMP 2009 - 2013 Summary & analysis of Results. Final Report.

Kondolf, G. M., Schmitt, R. J. P., Carling, P. A., Goichot, M., Keskinen, M., Arias, M. E., Bizzi, S., Castelletti, A., Cochrane, T. A., Darby, S. E., Kummu, M., Minderhoud, P. S. J., Nguyen, D., Nguyen, H. T., Nguyen, N. T., Oeurng, C., Opperman, J., Rubin, Z., San, D. C., … Wild, T. (2022). Save the Mekong Delta from drowning. Science, 376(6593), 583–585. https://doi.org/10.1126/science.abm5176

Landerer, F. W., Flechtner, F. M., Save, H., Webb, F. H., Bandikova, T., Bertiger, W. I., Bettadpur, S. V., Byun, S. H., Dahle, C., Dobslaw, H., Fahnestock, E., Harvey, N., Kang, Z., Kruizinga, G. L. H., Loomis, B. D., McCullough, C., Murböck, M., Nagel, P., Paik, M., … Yuan, D.-N. (2020). Extending the Global Mass Change Data Record: GRACE Follow-On Instrument and Science Data Performance. Geophysical Research Letters, 47(12), e2020GL088306. https://doi.org/10.1029/2020GL088306

Lehner, B., Liermann, C. R., Revenga, C., Vörösmarty, C., Fekete, B., Crouzet, P., Döll, P., Endejan, M., Frenken, K., Magome, J., Nilsson, C., Robertson, J. C., Rödel, R., Sindorf, N., & Wisser, D. (2011). High-resolution mapping of the world's reservoirs and dams for sustainable river-flow management. Frontiers in Ecology and the Environment, 9(9), 494–502. https://doi.org/10.1890/100125

Li, Y., Gao, H., Zhao, G., & Tseng, K.-H. (2020). A high-resolution bathymetry dataset for global reservoirs using multi-source satellite imagery and altimetry. Remote Sensing of Environment, 244, 111831. https://doi.org/10.1016/j.rse.2020.111831

Liang, J., Yang, Q., Sun, T., Martin, J. D., Sun, H., & Li, L. (2015). MIKE 11 model-based water quality model as a tool for the evaluation of water quality management plans. Journal of Water Supply: Research and Technology-Aqua, 64(6), 708–718. https://doi.org/10.2166/aqua.2015.048

Liang, X., Lettenmaier, D. P., Wood, E. F., & Burges, S. J. (1994). A simple hydrologically based model of land surface water and energy fluxes for general circulation models. Journal of Geophysical Research: Atmospheres, 99(D7), 14415–14428. https://doi.org/10.1029/94JD00483

Macian-Sorribes, H. (2017). Design of optimal reservoir operating rules in large water resources systems combining stochastic programming, fuzzy logic and expert criteria. Universitat Politècnica de València. Retrieved 8 June 2017 from https://doi.org/10.4995/THESIS/10251/82554.

Mu, Qiaozhen; Zhao, Maosheng; and Running, Steven W., "MODIS Global Terrestrial Evapotranspiration (ET) Product (NASA MOD16A2/A3) Collection 5. NASA Headquarters" (2013). Numerical Terradynamic Simulation Group Publications. 268. https://scholarworks.umt.edu/ntsg_pubs/268

Müller Schmied, H., Trautmann, T., Ackermann, S., Cáceres, D., Flörke, M., Gerdener, H., Kynast, E., Peiris, T. A., Schiebener, L., Schumacher, M., & Döll, P. (2023). The global water resources and use model WaterGAP v2.2e: Description and evaluation of modifications and new features. Geoscientific Model Development Discussions, 2023, 1–46. https://doi.org/10.5194/gmd-2023-213

MRC hydropower database. Mekong River Commission, 2017.

Mu, Qiaozhen; Zhao, Maosheng; and Running, Steven W., "MODIS Global Terrestrial Evapotranspiration (ET) Product (NASA MOD16A2/A3) Collection 5. NASA Headquarters" (2013). Numerical Terradynamic Simulation Group Publications. 268. https://scholarworks.umt.edu/ntsg_pubs/268

Pereira-Cardenal, S. J., Madsen, H., Arnbjerg-Nielsen, K., Riegels, N., Jensen, R., Mo, B., Wangensteen, I., & Bauer-Gottwein, P. (2014). Assessing climate change impacts on the Iberian power system using a coupled water-power model. Climatic Change, 126(3–4), 351–364.

Poff, N. L., Olden, J. D., Merritt, D. M., & Pepin, D. M. (2007). Homogenization of regional river dynamics by dams and global biodiversity implications. Proceedings of the National Academy of Sciences, 104(14), 5732–5737. https://doi.org/10.1073/pnas.0609812104

Pulido-Velazquez, M. A., Sahuquillo-Herraiz, A., Ochoa-Rivera, J. C., & Pulido-Velazquez, D. (2005). Modeling of stream-aquifer interaction: The embedded multireservoir model. Journal of Hydrology, 313(3–4). https://doi.org/10.1016/j.jhydrol.2005.02.026

Pulido-Velazquez, M., Perez-Martin, M. A., Solera, A., Collazos, G., Deidda, D., Alvarez-Mendiola, E., … Andreu, J. (2006). Desarrollo y aplicación de metodologías y herramientas en la cuenca piloto del río Júcar para los análisis económicos requeridos en la Directiva Marco Europea del Agua.

Sutanudjaja, E. H., van Beek, R., Wanders, N., Wada, Y., Bosmans, J. H. C., Drost, N., van der Ent, R. J., de Graaf, I. E. M., Hoch, J. M., de Jong, K., Karssenberg, D., López López, P., Peßenteiner, S., Schmitz, O., Straatsma, M. W., Vannametee, E., Wisser, D., & Bierkens, M. F. P. (2018). PCR-GLOBWB 2: A 5\,arcmin global hydrological and water resources model. Geoscientific Model Development, 11(6), 2429–2453. https://doi.org/10.5194/gmd-11-2429-2018

Tangi, M., Bizzi, S., Fryirs, K., & Castelletti, A. (2022). A Dynamic, Network Scale Sediment (Dis)Connectivity Model to Reconstruct Historical Sediment Transfer and River Reach Sediment Budgets. Water Resources Research, 58(2), e2021WR030784. https://doi.org/10.1029/2021WR030784

Terink, W., Lutz, A. F., Simons, G. W. H., Immerzeel, W. W., & Droogers, P. (2015). SPHY v2.0: Spatial Processes in HYdrology. Geoscientific Model Development, 8(7), 2009–2034. https://doi.org/10.5194/gmd-8-2009-2015

Trinh, N. X., Quang, T. T., Ha, P. D., Le Xuan, T., Dinh, C. D., Thanh, T. N., Quang, T. T., Duc, T. D., & Thanh, H. N. (2018). Delimitating inland aqua-ecological zones under different climate conditions in the Mekong Delta region, Vietnam. Journal of Water and Climate Change, 9(3), 463–479. https://doi.org/10.2166/wcc.2018.181

Turner, S. W. D., Steyaert, J. C., Condon, L., & Voisin, N. (2021). Water storage and release policies for all large reservoirs of conterminous United States. Journal of Hydrology, 603, 126843. https://doi.org/10.1016/j.jhydrol.2021.126843

van Beek, L. P. H., Wada, Y., & Bierkens, M. F. P. (2011). Global monthly water stress: 1. Water balance and water availability. Water Resources Research, 47(7). https://doi.org/10.1029/2010WR009791

van Jaarsveld, B., Wanders, N., Sutanudjaja, E. H., Hoch, J., Droppers, B., Janzing, J., van Beek, R. L. P. H., & Bierkens, M. F. P. (2024). A first attempt to model global hydrology at hyper-resolution. EGUsphere, 2024, 1–32. https://doi.org/10.5194/egusphere-2024-1025

Wada, Y., Wisser, D., & Bierkens, M. F. P. (2014). Global modeling of withdrawal, allocation and consumptive use of surface water and groundwater resources. Earth System Dynamics, 5(1), 15–40. https://doi.org/10.5194/esd-5-15-2014

Dams, data and decisions (2020): Water, Land and Ecosystems, [online] https://archive.iwmi.org/wle/thrive/2018/02/13/dams-data-and-decisions/.

Zhang, Y., Kong, D., Gan, R., Chiew, F. H. S., McVicar, T. R., Zhang, Q., & Yang, Y. (2019). Coupled estimation of 500 m and 8-day resolution global evapotranspiration and gross primary production in 2002–2017. Remote Sensing of Environment, 222, 165–182. https://doi.org/10.1016/j.rse.2018.12.031

Zheng, C., Jia, L., & Hu, G. (2022). Global land surface evapotranspiration monitoring by ETMonitor model driven by multi-source satellite earth observations. Journal of Hydrology, 613, 128444. https://doi.org/10.1016/j.jhydrol.2022.128444

Ziv, G., Baran, E., Nam, S., Rodríguez-Iturbe, I., & Levin, S. A. (2012). Trading-off fish biodiversity, food security, and hydropower in the Mekong River Basin. Proceedings of the National Academy of Sciences, 109(15), 5609–5614. https://doi.org/10.1073/pnas.1201423109

SIWRP (2021), Master plan study on irrigation and risk reduction for the period 2021-2030, vision to 2050. Hydraulic report for the Mekong delta.

SIWRP (2021), Master plan study on irrigation and risk reduction for the period 2021-2030, vision to 2050. Hydrology and water resources report for the Mekong delta.

Disclaimer

Acknowledgement of funding

Funded by the European Union

This project has received funding from the European Union's Horizon Europe research and innovation programme under grant agreement No 101059264.

Annex I

Table of Figures

Figure 1: Depicts the basin boundaries of the Danube River Basin. The Danube River is shown in blue, while the upper basin is outlined in black. 10
Figure 2: Components of the hydrological cycle and the water management process simulated in CWatM 11
Figure 3: Jucar river basin location map 12
Figure 4: Schematic of the Jucar river hydro-economic model 13
Figure 5: Mekong River basin location map 15
Figure 6: Schematic showing the coupling between Vic-Res using the combined rainfall-runoff model and the routing model 16
Figure 7: The figure shows VRSAP model network in the Mekong delta. Nodes are shown in black and the necessary linkages are shown in red, pink, green, and blue 18
Figure 8: Map of the Rhine Catchment obtained from Moser et al (2018) 19
Figure 9: Schematic drawing of a the human water use components in PCRGLOBWB 2 from Wada et al., 2014. 20
Figure 10: Workflow of Species Distribution Models 21
Figure 11: Schematic overview of the D-CASCADE model from Tiang et al., 2022. 23
Figure 12: Layout of SIWRP's Mike11 model of the Mekong delta. 24
Figure 13: Integration of the output of the hydrological models as environmental variables for species distribution models as an approach to improve the habitat suitability predictions of freshwater biodiversity 25
Figure 14: Schematic that shows the hard coupling between Vic-Res and the sediment transport model: D-CASCADE 26
Figure 15: Linkage of Mekong delta models and upstream Mekong models 27
Figure 16: Location map of hydrological stations in the Mekong delta for model calibration 33
Figure 17: Calibration results (KGE) for the Danube of 581 calibration stations 35
Figure 18: Correlation between GloLakes and examples of reservoir storage simulated with CWatM 35
Figure 19: KGE cumulative distribution of the ETa simulated with CWatM vs. remote sensing products. 36
Figure 20: Reservoir storages comparison plots between the Jucar hydro-economic model and observations 38
Figure 21: Reservoir releases comparison plots between the Jucar hydro-economic model and observations 39
Figure 22: Streamflow comparison plots between the Jucar hydro-economic model and observations 41
Figure 23: Demand delivery comparison plots between the Jucar hydro-economic model and observations 43
Figure 24: Albufera water balance comparison between the Jucar hydro-economic model and the Jucar RBA model 44
Figure 25: Observed and simulated hydrographs at Stung Treng 45

Figure 26: Observed and simulated hydrographs at Chiang Saen, Vientiane, Mukdahan, and Pakse . 46
Figure 27 On the left panel we show the map of geomorphic regions shown in the same color scheme of the right panel and including their estimated annual sediment yields. On the right panel we illustrate the charts showing the average annual composition of the delivered sediment. 47
Figure 28: Validation of VRSAP model for flood flow water level (1 July to 30 November) at upper station (Tan Chau) 49
Figure 29: Validation of VRSAP model for dry flow water level (1 February to 30 April) at upper station (Tan Chau) 49
Figure 30: Validation of VRSAP model for dry flow discharge at main river mouth 50
Figure 31: Cumulative density plot of the monthly KGE values in the Rhine basin. Lines are colored by the model used..... 52
Figure 32: Panel plot of the difference between the Turn250 and BaseGeoDAR models and the Baseline model for the three components of KGE: correlation (a), bias ratio (b), and variance ratio (c). 53
Figure 33: Line plot showing the different models: Turn250 (pink), BaseGeoDAR (grey) and Baseline (black) against GRDC observations (dashed black) at Lobith, NL for a dry year (a) and a normal year (b). 54
Figure 34: Flow duration curves (FDC) for all three models: Turn250 (pink), BaseGeoDAR (grey) and Baseline (black) and GRDC observations (black dashed), at three locations along the Rhine (Lobith, NL for the lower Rhine, Andernach, DE for the middle Rhine, and Basel Rheinhalle, CH for the upper Rhine). 54
Figure 35 Depicts the long term average monthly reservoir storage fraction across the European continent for three model runs (Baseline in black, BaseGeoDAR in grey, and Turn250 in pink)..... 55
Figure 36: Depicts long term montlhy average reservoir storage fraction in the Rhine basin for all three models: Turn250 in pink, BaseGeoDAR in grey, and Baseline in black, against modelled values in GloLakes (dashed black) (Hou et al., 2024). 56
Figure 37: Depicts the annual total water storage in the Rhine basin for the Turn250 (pink) and the Baseline (black) models on the left axis. The right axis depicts the liquid water equivalent (LWE) in GRACE-FO in dashed blue..... 56
Figure 38: Habitat suitability maps for four species in the Danube Basin, all of them having different habitat suitability distribution patterns along the river network. 58
Figure 39: Habitat suitability maps for four species in the Júcar Basin, all of them having different habitat suitability distribution patterns along the river network. 59
Figure 40: Geographical patterns of species habitat richness, understanding high richness areas (i.e., dark red colors) as areas where high suitability values were found for most species analyzed. 60
Figure 41: Habitat suitability maps for four species in the Rhine Basin, all of them having different habitat suitability distribution patterns along the river network. 61
Figure 42: Habitat suitability maps for four species in the Rhine Basin, all of them having different habitat suitability distribution patterns along the river network. 62
Figure 43: Habitat suitability maps for three species in the southern section of the Mekong Basin, all of them having different habitat suitability distribution patterns along the river network. 63